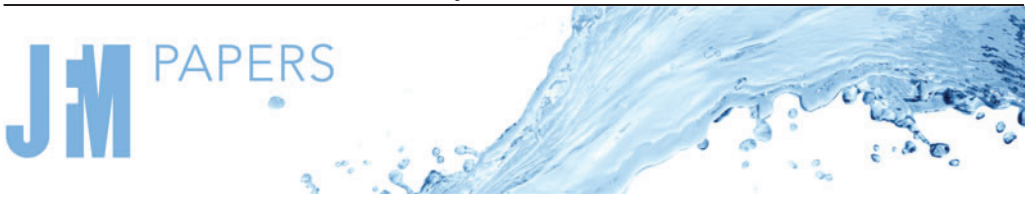
J. Fluid Mech. (2022), *vol*. 941, A35, doi:10.1017/jfm.2022.293



Drag-related wave–current interaction inside a dense submerged aquatic canopy

Weikai Tan[1,2] **and Jing Yuan**[1,†]

[1]State Key Laboratory of Hydroscience and Engineering, Department of Hydraulic Engineering, Tsinghua University, Beijing 100084, PR China

[2]Huawei Technologies Co., Ltd., Huawei Industrial Park, Bantian, Longgang District, Shenzhen 518129, PR China

(Received 10 June 2021; revised 8 March 2022; accepted 23 March 2022)

The seabed in coastal regions is often covered by a dense submerged canopy formed by benthic organisms. The in-canopy flow is of great interest to coastal researchers. In this study, a semi-analytical model is proposed for the in-canopy current profile under the influence of coexisting waves. The current is driven by a mean shear stress at the canopy top and a mean streamwise pressure gradient. Wave–current interaction arises from the mean canopy drag, which is described by the conventional quadratic law. An algebraic eddy viscosity model, which accounts for the turbulence generated by a canopy-scale vortex and stem-scale wake, is proposed. The model is calibrated against unidirectional flume experiments, and is subsequently validated against a wave–current flume experiment. It is found that the mean canopy drag experienced by the current can be significantly amplified by a co-existing wave-driven oscillatory flow. Under the same current driving force, the current in wave–current flow is reduced from that in a pure-current flow. The reduction increases with canopy density and wave strength. For a wave and current at an angle, veering of the current velocity vector is suggested by the model, which makes the mean canopy drag align with the driving force of the current.

Key words: turbulent boundary layers, coastal engineering

1. Introduction

Many sessile benthic organisms in coastal regions form rough seabed surfaces resembling submerged dense canopies, e.g. seagrass meadows and the coral communities. Their presence plays a significant role in many physical coastal processes, e.g. wave attenuation (Suzuki *et al.* 2012; Ma *et al.* 2013; Hu *et al.* 2014) and sediment deposition (Ward, Kemp & Boynton 1984; Donatelli *et al.* 2018). Coastal waves and currents also affect

† Email address for correspondence: yuanj2021@mail.tsinghua.edu.cn

© The Author(s), 2022. Published by Cambridge University Press

https://doi.org/10.1017/jfm.2022.293 Published online by Cambridge University Press

the biological processes of benthic organisms by influencing primary production, nutrient uptake, larva settlement and mass transport inside the canopies (Carpenter, Hackney & Adey 1991; Hurd 2000; Falter, Atkinson & Coimbra 2005; Reidenbach, Koseff & Koehl 2009). Understanding the characteristics of in-canopy flow is the prerequisite for interpreting and modelling the complex mechanisms of flow–canopy interactions (Adams *et al.* 2018) and developing eco-engineering methods (e.g. restoration and transplantation of coral or seagrass) for coastal protection (Ferrario *et al.* 2014; Ondiviela *et al.* 2014). Classifications of canopy flow are mainly based on submergence (the ratio of water depth, h, to canopy height h_c) and solidity (the ratio of the frontal area of the canopy and the bed area). Coastal aquatic canopies are usually classified as submerged ($h/h_c > 1$) and dense (high solidity) canopies (later discussed in § 2.1.1).

Many previous studies focused on unidirectional flows in a submerged canopy, which are driven by a streamwise pressure gradient (due to e.g. bed slope) and the shear at the top of canopy (Nepf & Vivoni 2000). The flow inside a dense canopy is significantly retarded due to the strong canopy drag. This leads to a drag discontinuity at the canopy top, creating a region resembling a free shear layer (Raupach, Finnigan & Brunet 1996), in which canopy-scale Kelvin–Helmholtz (KH) vortices are generated due to a very strong vertical shear. These canopy-scale vortices control the mass transport and turbulence mixing in the upper part of a canopy (Ghisalberti & Nepf 2002; Dupont & Brunet 2009). In-canopy turbulence can also be produced by the interaction between the flow and an individual stem or blade of the canopy, e.g. the turbulence wake and vortex generated behind a rigid stem (Tanino & Nepf 2008*a*). This small-scale turbulence also contributes to mobilizing and suspending sediment inside a canopy (Tinoco & Coco 2018; Yang & Nepf 2018). For a dense canopy, the penetration depth of KH vortices, δ_P, is smaller than the canopy height, h_c, so the entire canopy is separated into two parts. The upper layer ($h_c - \delta_P < z \leq h_c$, z is vertical coordinate) is driven by the turbulent Reynolds stress and pressure gradient, and the strong canopy-scale turbulence is dominant. The lower layer ($0 \leq z \leq h_c - \delta_P$, $z = 0$ is the bottom) is controlled by the weak stem-scale turbulence, and a balance between drag and pressure forces is established, leading to a nearly depth-uniform flow velocity. Thus, predictive models of unidirectional flow in a dense submerged canopy must consider both layers and turbulence generated at both scales. Ghisalberti & Nepf (2004) proposed a one-dimensional numerical model for unidirectional flow in a submerged rigid dense canopy. This model adopts a constant velocity in the lower layer and a mixing length model for quantifying the canopy-scale Reynolds stress in the upper layer. King, Tinoco & Cowen (2012) proposed a $k - \epsilon$ (turbulent kinetic energy – dissipation) turbulence closure model, which separately models the turbulence produced by shear and the stem wake. These models are able to give a velocity profile with an inflection point near the top of the canopy, which is the key feature of such flows.

For unidirectional canopy flow, which is also relevant to the atmospheric boundary layer over a forest, there are many numerical studies that treat the canopy as a continuous medium, so some parameterizations are proposed to account for canopy drag in momentum and turbulence closure models (see the review by Viana Parente Lopes, Palma & Silva Lopes 2021). In recent years, some numerical studies, which can directly resolve individual canopy elements, have been reported. For instance, Zhou & Venayagamoorthy (2019) used large eddy simulation (LES) to study the flow through a cylindrical canopy patch suspended in deep water. Monti *et al.* (2020) used immersed boundary method (IBM) in LES modelling of open-channel flow over submerged canopy (array of rods) with a variety of submergences. Tschisgale *et al.* (2021) applied the LES–IBM combination to a flexible canopy. These direct numerical simulations can reveal

https://doi.org/10.1017/jfm.2022.293 Published online by Cambridge University Press

the detailed spatial-temporal variation of in-canopy flow, and hence were used to better understand coherent structures generated under various flow and canopy conditions.

The majority of research on wave–vegetation interaction focused on the wave height attenuation (e.g. Fonseca & Cahalan 1992; Mendez & Losada 2004; Luhar, Infantes & Nepf 2017). In recent years, researchers began to investigate the detailed in-canopy hydrodynamics, and the main research findings are as follows. First, the wave-induced oscillatory flow is much less attenuated than current-induced unidirectional flow inside a canopy (e.g. Lowe, Koseff & Monismith 2005; Weitzman *et al.* 2015; Zeller *et al.* 2015). This is because wave produces an oscillatory pressure gradient as the main driver for in-canopy flow. This pressure gradient is mainly balanced by the inertial force, which is comparable to or even larger than the canopy drag, so the in-canopy flow is not significantly attenuated. Second, a wave can produce a mean flow inside the canopy. Progressive waves transfer momentum into a submerged canopy and generate a mean Eulerian in-canopy flow, which is similar to the wave boundary layer streaming over a flat bottom. This phenomenon is observed in flume experiments (e.g. Luhar *et al.* 2010; Abdolahpour, Hambleton & Ghisalberti 2017) or field studies (e.g. Luhar *et al.* 2013). Luhar *et al.* (2010) developed a simple depth-averaged model, which gives a sizeable wave-driven mean flow. van Rooijen *et al.* (2020) numerically showed that the in-canopy mean flow is forced by both wave stress and Reynolds stress at the canopy top. Third, the turbulence of oscillatory in-canopy flows is studied by some researchers. Ghisalberti & Schlosser (2013) showed that oscillatory flows, similar to unidirectional flows, can generate coherent vortices at the top of the submerged canopy, if the excursion amplitude and the Reynolds number of the oscillatory flow are sufficiently large. Zhang, Tang & Nepf (2018) experimentally showed that the stem-scale turbulence of oscillatory in-canopy flows becomes significant if the ratio A_w/s is over 0.5, where A_w is the excursion amplitude of the oscillatory flow and s is the stem spacing.

Coastal regions have co-existing waves and currents, but the research on wave–current flow inside a submerged canopy is rather limited. Some recent studies investigated wave–current canopy flow through numerical simulations (Li & Yan 2007; King *et al.* 2012; Maza, Lara & Losada 2013; Zeller *et al.* 2015), but these studies mainly focused on model development. Lou *et al.* (2018) conducted a wave flume experiments involving wave–current flows. They found that the presence of waves reduced the in-canopy current velocity, and they attributed this to the presence of a wave-induced mean flow. Chen *et al.* (2020) studied the stem-scale turbulence under wave–current flows through flume experiments. Nonlinear wave–current interaction inside a turbulent benthic boundary layer is well known (see Grant & Madsen 1986). For instance, the nonlinear nature of the turbulent Reynolds stress allows the turbulence generated by waves to significantly affect the current profile in the boundary layer (e.g. Grant & Madsen 1979; Yuan & Madsen 2015). Thus, an immediate question is whether a nonlinear wave–current interaction also exists for in-canopy flows.

There are a number of factors that can possibly lead to strong wave–current interactions, such as the movement of flexible canopy element, the Eulerian mean flow driven by wave, the nonlinearity of turbulent Reynolds stress, etc. Each of these factors may be the dominant one under certain circumstances, but before we build a comprehensive model, it is desirable to first investigate each factor separately. Here, we choose to study the drag-related wave–current interaction. The in-line drag force on a cylinder is often modelled using a quadratic law, i.e. $F_D \propto u^2$, where u is flow velocity. If this law is applied to give the instantaneous drag force under wave–current flow using the instantaneous

https://doi.org/10.1017/jfm.2022.293 Published online by Cambridge University Press

velocity, $u(t)$, the time-averaged drag force is then proportional to $\overline{u(t)^2}$ (overline indicates time averaging). Since $\overline{u(t)^2}$ is not necessarily equal to $\overline{u(t)}^2$, the drag force experienced by the current is thus modified by co-existing waves. This effect, if indeed it is significant, must be accounted for in any coastal canopy–flow model, regardless of the canopy type.

In this paper, a one-dimensional semi-analytical model is developed for the current velocity profile inside a dense submerged canopy, which can account for a coexisting oscillatory flow driven by waves. Here, we only consider the wave's effect on the current. The main reason is that the in-canopy current is more important for understanding the transport of nutrients, sediment and mass in a canopy. Also, some existing laboratory experiment, e.g. Lou *et al.* (2018), showed that the wave-induced oscillatory flow is not heavily changed by adding a current. The validated model is subsequently used to illustrate the effects of waves on currents in a submerged canopy. The outline of the paper is as follows. Section 2 presents the semi-analytical model. Section 3 shows model validation. The discussions on currents in a submerged canopy with waves are provided in § 4, and conclusions are provided in § 5.

2. Model description

This section presents a one-dimensional vertical (1-DV) model for currents in a dense submerged canopy with a co-existing oscillatory flow produced by surface waves. We first outline the idealized problem and state the model assumptions. The governing equations and boundary conditions are then provided. The closure models for time-averaged Reynolds stress and canopy drag are subsequently presented. Finally, the solution of current velocity profile is outlined.

2.1. *Idealization*

The field condition can be quite complicated due to the complexity of the canopy morphology, the detailed behaviour of shoaling waves and overlying current. Here, we choose to idealize the problem as a horizontal flow passing an array of cylinders, which allows us to focus on the drag-related effect. Some assumptions are imposed, which cover three aspects: canopy, wave and current. A sketch is provided in figure 1 to facilitate the following introductions. A summary of the assumptions is provided in table 1.

2.1.1. *Idealization of canopy*

The canopy is simplified as an array of uniform rigid cylinders with a diameter, d, a canopy height, h_c, and a uniform spacing among canopy elements, s. Another important parameter of the canopy is the front area per unit volume, $a = d/s^2$. For a cylindrical canopy element, the solid volume fraction of the canopy, ϕ, can be approximated as $\phi = \pi ad/4$ (Nepf 2012). Strictly speaking, the arrangement of the cylinders, e.g. staggered or grid arrangement, may affect the hydrodynamic characteristics of the canopy, but here we neglect this influence and assume the canopy is an isotropic (any parameter of the canopy is not a function of flow direction) and homogeneous medium. This is acceptable under the assumption of low solid volume fraction, i.e. $\phi \ll 1$.

We would like to have a dense canopy, such that the KH vortices cannot fully penetrate the whole canopy. According to Ghisalberti (2009), the penetration depth of KH vortices

https://doi.org/10.1017/jfm.2022.293 Published online by Cambridge University Press

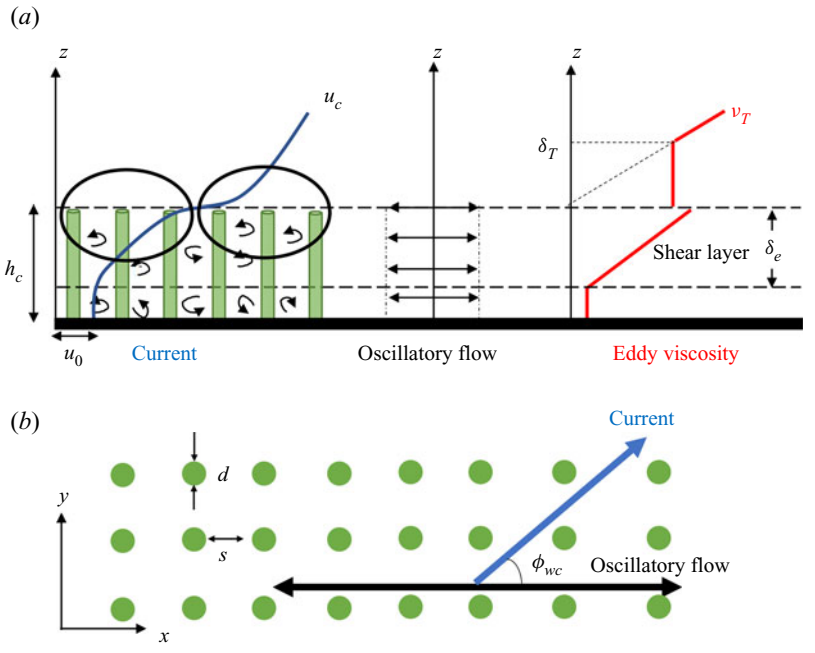


Figure 1. Schematic sketch of wave–current flows in a dense submerged canopy. (*a*) Side view, (*b*) top view.

Assumptions	Realization/parameter range
Canopy	
Low solid volume fraction	$ad \ll 1$ or $\phi \ll 1$
Rigid body	Rigid cylinders as idealized canopy elements
Isotropic and homogeneous	constant (a, h_c, d), ignore the pattern of placements
Sufficiently dense	$\hat{a} = ah_c > 0.2$
Sufficiently submerged	$h/h_c - 1$ is at least close to 1
Wave	
Depth-uniform oscillatory flow	Moderate value for A_w/s (e.g. <10)
Current does not affect wave	$\hat{u}_w$ is not modelled
No vertical velocity	Vertical velocity is zero
Wave-induced mean flow is negligible	$\hat{\tau}_w \ll 1$ (3.7)
Current	
1-DV problem	$\hat{u}_c$ is a function of $\hat{z}$
Flow is turbulent dominated	Ignore viscous stress

Table 1. Summary of assumptions and parameter ranges of the proposed model.

for a submerged canopy is

$$\delta_p = \frac{0.23}{C_D a}, \tag{2.1}$$

where C_D is a drag coefficient (close to 1). By requiring $\delta_p < h_c$, (2.1) gives that the solidity, $\hat{a} = ah_c$, must satisfy $\hat{a} > 0.23/C_D$. Note that 0.23 is an empirical number obtained by fitting some measurements, so we expect the solidity to be over 0.2 to satisfy

https://doi.org/10.1017/jfm.2022.293 Published online by Cambridge University Press

the requirement of a dense canopy. This can be achieved by having a tall canopy or a relatively high solid volume fraction.

Another assumption is that the canopy should be sufficiently submerged, e.g. the water depth should be at least comparable to (preferably much larger than) the canopy height. This assumption is required for treating wave-induced flow as a bottom-parallel oscillation. Also, it allows us to neglect the influence of surface processes on the in-canopy flow.

2.1.2. *Idealization of wave*

The wave-driven in-canopy flow, u_w, is approximated as an oscillatory flow with a sinusoidal temporal variation, i.e.

$$u_w = U_w \cos(\omega t), \tag{2.2}$$

where t is time, U_w is the amplitude and $\omega = 2\pi/T$ is the radian frequency of the oscillatory flow, with T being the flow period. Many flume experiments (e.g. Lowe *et al.* 2005) showed that the oscillatory in-canopy flow can be fairly depth uniform. According to Ghisalberti & Schlosser (2013), a significant shear of the oscillatory velocity profile, which is due to the generation of a coherent vortex at the canopy top, only exists if the Keulegan–Carpenter number, $KC = U_w T/L_D$, is sufficiently large (they proposed $KC = 5$ as an indicative threshold). Here, L_D is a drag length scale defined as

$$L_D = \frac{1-\phi}{C_D a}, \tag{2.3}$$

where C_D is the canopy drag coefficient (discussed in § 2.4). For typical aquatic canopies, $C_D \approx 1$ and $\phi \ll 1$, so $KC \approx 2\pi(d/s)A_w/s$. Note that d/s is much smaller than 1 under the requirement of $\phi \ll 1$, so KC can be comparable to or less than 5 for A_w/s less than 10. This means that an oscillatory flow, for which the excursion amplitude does not far exceed the element spacing, can be approximated as a depth-uniform oscillatory flow inside the canopy. The previous flume experiments usually have A_w/s comparable to or less than 1. For typical coastal benthic canopies (e.g. coral reefs or seagrass meadows), for which s is of $O(1\,\mathrm{cm})$, A_w/s can still be less than 10 under typical wave conditions, e.g. a wave of 50 cm height and 3 s period gives $A_w = 12\,\mathrm{cm}$ at a seabed that is 3 m below the mean sea level. We here restrict our model application to waves that give a moderate or small A_w/s, so a depth-invariant oscillatory flow can be assumed inside the canopy. With this limitation, the in-canopy oscillatory flow does not generate canopy-scale vorticity/turbulence, but still produces stem-wake turbulence. This is important for the parameterization of turbulent eddy viscosity in § 2.4. The model also neglects the vertical wave-induced orbital velocity, so the wave-induced mean Eulerian flow, for which an important driver is the wave stress at the top of the canopy, is omitted. Some discussions on this approximation will be presented in § 3.2. As previously mentioned, we only consider the wave's effect on the current, so the oscillatory in-canopy flow is assumed to be constant, and is taken as a model input.

2.1.3. *Idealization of current*

The current is taken as a horizontal flow at an angle to the axis of the oscillatory flow. The positive oscillatory flow direction is taken as the x-direction (see figure 1), so the current

https://doi.org/10.1017/jfm.2022.293 Published online by Cambridge University Press

velocity, which is at an angle, ϕ_{wc}, to the x-direction is defined as

$$\boldsymbol{u}_c = (u_{cx}, u_{cy}) = u_c(\cos\phi_{wc}, \sin\phi_{wc}). \tag{2.4}$$

We assume the current is uniform in the $x-y$ plane, so the problem is reduced to a 1-DV problem, The combined flow velocity inside the canopy can therefore be written as

$$\boldsymbol{u}(z,t) = \left(U_w\cos(\omega t) + u_{cx}(z), u_{cy}(z)\right), \tag{2.5}$$

where z is the vertical coordinate with $z=0$ being the bottom. The current is driven by a shear stress at the top of the canopy, $\boldsymbol{\tau}_h = (\tau_{hx}, \tau_{hy})$, and a gradient, $\boldsymbol{S} = (S_x, S_y)$. For a fully developed open-channel current with a water depth, h, the relative importance of $\boldsymbol{\tau}_h$ over $\boldsymbol{S}$ is represented by the ratio (Nepf 2012)

$$\frac{\textit{shear stress}}{\textit{pressure gradient}} \sim \frac{|\boldsymbol{\tau}_h|}{gh_c|\boldsymbol{S}|} = \frac{h}{h_c} - 1, \tag{2.6}$$

where g is the gravitational acceleration. For deeply submerged flow ($h/h_c \gg 1$), $\boldsymbol{\tau}_h$ is the dominant driving force, and $\boldsymbol{S}$ can be neglected. In such cases, $\boldsymbol{\tau}_h$ can also be taken as the current bottom shear stress experienced by the overlying flow. The in-canopy current is subject to a time-averaged Reynolds stress and canopy drag. In our model, the time-averaged Reynolds stress is given as the product of a turbulent eddy viscosity, ν_T, and current velocity gradient, i.e.

$$\frac{\tau_i}{\rho} = \nu_T\frac{\partial u_{ci}}{\partial z}, \quad i = x, y. \tag{2.7}$$

Here, we ignore the viscous stress, since it is much weaker than the Reynolds stress in typical field conditions and also the laboratory conditions covered in this study. The instantaneous drag force is modelled using the conventional quadratic drag law adopted by many other researchers, so the time-averaged drag force, $\boldsymbol{f}_d$, is written as

$$\boldsymbol{f}_d = (f_{dx}, f_{dy}) = \tfrac{1}{2}C_D a\overline{|\boldsymbol{u}(z,t)|\boldsymbol{u}(z,t)}, \tag{2.8}$$

where the overline denotes time averaging.

2.2. *Governing equations*

The governing equations for u_{cx} and u_{cy} inside the submerged canopy are

$$\left.\begin{aligned}\frac{\partial}{\partial z}\left(\nu_T\frac{\partial u_{cx}}{\partial z}\right) &= -gS_x + f_{dx},\\ \frac{\partial}{\partial z}\left(\nu_T\frac{\partial u_{cy}}{\partial z}\right) &= -gS_y + f_{dy}.\end{aligned}\right\} \tag{2.9}$$

In this study, a current is prescribed by the canopy-top shear stress, $\boldsymbol{\tau}_h$ and the pressure gradient $\boldsymbol{S}$. With the closure models of ν_T and (f_{dx}, f_{dy}), (2.9) can be solved with two bottom boundary conditions.

Since we assume a dense canopy, the penetration depth of the canopy-scale shear layer is less than the canopy height, so there is a near-bed layer in which the in-canopy current

https://doi.org/10.1017/jfm.2022.293 Published online by Cambridge University Press

is almost depth uniform. Therefore, a zero-gradient bottom boundary condition for current velocity is adopted

$$\frac{\partial u_{ci}}{\partial z} = 0, \quad \text{at } z = 0,\ i = x,\ y. \tag{2.10}$$

This boundary condition also means that the bottom shear stress is ignored, and the model does not resolve the bottom boundary layer in the immediate vicinity of the bed. Therefore, the no-slip boundary condition is no longer applicable, and is replaced by a slip boundary condition

$$\boldsymbol{u}_c = \boldsymbol{u}_0 = (u_{0x}, u_{0y}) \quad \text{at } z = 0, \tag{2.11}$$

where $\boldsymbol{u}_0$ is the uniform in-canopy current velocity below the penetration depth. The value of $\boldsymbol{u}_0$ is iteratively determined by requiring that the obtained u_{cx} and u_{cy} profiles give the prescribed $\boldsymbol{\tau}_h$ at the canopy top, i.e.

$$\nu_T \frac{\partial u_{ci}}{\partial z}\bigg|_{z=h_c} = \frac{\tau_{hi}}{\rho}, \quad i = x, y. \tag{2.12}$$

To better reveal the underlying physics and identify the dimensionless parameters controlling the in-canopy current, the governing equations are normalized. Here, we choose the shear velocity associated with $\boldsymbol{\tau}_h$ as the representative velocity

$$u_{*c} = \sqrt{\frac{|\boldsymbol{\tau}_h|}{\rho}}, \tag{2.13}$$

because $\boldsymbol{\tau}_h$ represents a key driving force for the in-canopy current, and it is also the resistance experienced by the flow above the submerged canopy. The flow velocity is normalized by u_{*c}

$$\hat{\boldsymbol{u}} = \frac{\boldsymbol{u}}{u_{*c}}, \quad \hat{u}_w = \frac{U_w}{u_{*c}}, \quad \widehat{\boldsymbol{u}_c} = (\hat{u}_{cx}, \hat{u}_{cy}) = \left(\frac{u_{cx}}{u_{*c}}, \frac{u_{cy}}{u_{*c}}\right). \tag{2.14a–c}$$

The vertical coordinate is normalized by the canopy height

$$\hat{z} = \frac{z}{h_c}. \tag{2.15}$$

The turbulence eddy viscosity is normalized by the product of u_{*c} and h_c

$$\hat{\nu}_T = \frac{\nu_T}{u_{*c} h_c}. \tag{2.16}$$

The pressure gradients, gS_x and gS_y, are normalized by u_{*c}^2/h_c

$$\hat{\boldsymbol{S}} = \left(\hat{S}_x, \hat{S}_y\right) = \left(\frac{g h_c S_x}{u_{*c}^2}, \frac{g h_c S_y}{u_{*c}^2}\right). \tag{2.17}$$

The canopy drag is normalized by u_{*c}^2/h_c

$$(\hat{f}_{dx}, \hat{f}_{dy}) = \frac{(f_{dx}, f_{dy})}{u_{*c}^2/h_c} = \frac{1}{2} C_D \hat{a} \hat{u}_c^2 (\beta_{cx}, \beta_{cy}), \tag{2.18}$$

where

$$\hat{a} = a h_c \tag{2.19}$$

https://doi.org/10.1017/jfm.2022.293 Published online by Cambridge University Press

is the solidity of the canopy, and β_{cx} and β_{cy} are defined as

$$(\beta_{cx}, \beta_{cy}) = \frac{\overline{|\hat{\boldsymbol{u}}(z,t)|\hat{\boldsymbol{u}}(z,t)}}{\hat{u}_c^2}. \tag{2.20}$$

Note that $\beta_c = \sqrt{\beta_{cx}^2 + \beta_{cy}^2} = 1$ for current-alone cases, so the value of β_{ci} allows us to quantify the wave's effect on the mean drag experienced by the current, which will be discussed in § 2.4. The normalized governing equations are

$$\left.\begin{aligned} \frac{\partial}{\partial \hat{z}}\left(\hat{\nu}_T \frac{\partial \hat{u}_{cx}}{\partial \hat{z}}\right) &= -\hat{S}_x + \hat{f}_{dx}, \\ \frac{\partial}{\partial \hat{z}}\left(\hat{\nu}_T \frac{\partial \hat{u}_{cy}}{\partial \hat{z}}\right) &= -\hat{S}_y + \hat{f}_{dy}. \end{aligned}\right\} \tag{2.21}$$

The normalized bottom boundary conditions are

$$\hat{\boldsymbol{u}}_c = (\hat{\boldsymbol{u}}_{0x}, \hat{\boldsymbol{u}}_{0y}) = \left(\frac{u_{0x}}{u_{*c}}, \frac{u_{0y}}{u_{*c}}\right), \quad \text{at } \hat{z} = 0, \tag{2.22}$$

and

$$\frac{\partial \hat{u}_{ci}}{\partial \hat{z}} = 0, \quad \text{at } \hat{z} = 0,\ i = x, y. \tag{2.23}$$

The normalized solution must satisfy

$$\left(\hat{\nu}_T \frac{\partial \hat{u}_{cx}}{\partial \hat{z}}, \quad \hat{\nu}_T \frac{\partial \hat{u}_{cy}}{\partial \hat{z}}\right) = (\cos\phi_{\tau h}, \ \sin\phi_{\tau h}), \quad \text{at } \hat{z} = 1, \tag{2.24}$$

where $\phi_{\tau h}$ is the angle between $\boldsymbol{\tau}_h$ and the x-direction.

2.3. *Turbulent eddy viscosity*

For current in a dense submerged canopy, turbulence is generated around the top of the canopy due to a strong local vertical shear (hereafter referred to as shear turbulence) and in the stem wake (hereafter referred to as wake turbulence). The shear turbulence is at the canopy scale, while the wake turbulence is at the stem scale. We follow King *et al.* (2012) to parameterize the turbulent eddy viscosity inside the canopy as the sum of two components corresponding to the two types of turbulence.

In the $k - \epsilon$ turbulence closure model of King *et al.* (2012), the wake-turbulence-related eddy viscosity is given by

$$\nu_w = C_\lambda \frac{k_w^2}{\epsilon_w}, \tag{2.25}$$

where C_λ is a constant, k_w is the kinetic energy of wake turbulence and ϵ_w is the dissipation rate of wake turbulence. Following Tanino & Nepf (2008*b*), ϵ_w is given by

$$\epsilon_w = C_{\epsilon D} \frac{k_w^{3/2}}{d}, \tag{2.26}$$

where $C_{\epsilon D}$ is a constant. By substituting (2.26) into (2.25), we get

$$\nu_w = \frac{C_\lambda}{C_{\epsilon D}} \sqrt{k_w} d, \tag{2.27}$$

where Zhang *et al.* (2018) showed that k_w in oscillatory flow can be modelled using the wake turbulent kinetic energy (TKE) model of Tanino & Nepf (2008*b*). For a small solid

https://doi.org/10.1017/jfm.2022.293 Published online by Cambridge University Press

volume fraction, this model can be approximately written as

$$\sqrt{k_w} \approx \delta \left(\tfrac{1}{2} C_D a d\right)^{1/3} U_r, \tag{2.28}$$

where δ is a model constant and U_r is a reference velocity. By substituting (2.28) into (2.27), we get

$$\nu_w = \left[\delta \frac{C_\lambda}{C_{\epsilon D}} \left(\frac{1}{2} C_D\right)^{1/3}\right] (ad)^{1/3} U_r d = c_w (ad)^{1/3} U_r d. \tag{2.29}$$

King *et al.* (2012), through model calibration, obtained $C_\lambda = 0.01$ and $C_{\epsilon D} = 0.2795$. Zhang *et al.* (2018), through fitting measurements, obtained that $\delta = 0.76$, and they assumed $C_D = 1.4$. Using these parameters, the value of c_w is 0.024. We are aware that it is better to calibrate c_w using existing experimental results, but we found that the model's performance (in terms of predicting the in-canopy current) weakly depends on the value of c_w. This is mainly because ν_w is only important in the very near-bed region, but the Reynolds stress in this region is negligible compared with the canopy drag and pressure gradient. Since another calibration parameter is introduced in the shear-related eddy viscosity (discussed later), we decided to simple accept the value $c_w = 0.024$, so the model calibration process was simplified. We have conducted a sensitivity analysis for c_w, and found that the prediction changes by only a few per cent even if c_w is doubled (taking $c_w = 0.048$).

The representative velocity for wave–current flow is taken as the root-mean-square (r.m.s.) velocity near the bottom of the canopy, i.e.

$$U_r = \sqrt{\frac{1}{2} U_w^2 + |\boldsymbol{u}_0|^2}. \tag{2.30}$$

Choosing the r.m.s. velocity is to include wake turbulence generated by both oscillatory and current flows. A conventional representative velocity of the oscillatory flow is its velocity amplitude, U_w. For the current, $|\boldsymbol{u}_0|$, which is the magnitude of the current velocity at the bottom of the canopy, is taken as the representative velocity. This is because the contribution of wake turbulence is most important in the lower part of the canopy, so using $|\boldsymbol{u}_0|$ means that U_r represents the local flow. In the upper part of the canopy, the local current velocity is much stronger than $|\boldsymbol{u}_0|$, so the proposed U_r is smaller than the local r.m.s. velocity. This should not lead to a big model error, because ν_w is much smaller than the shear-related eddy viscosity, ν_s, in the upper part of the canopy.

The parameterization of ν_s is based on the flume experimental results of Ghisalberti & Nepf (2004), who studied unidirectional flow in a submerged dense canopy. In their study, ν_s was estimated from measured shear and Reynolds stress. They found that ν_s increases from the bottom of shear layer, i.e. $z_1 = h_c - \delta_e$, where δ_e is the depth of the region with a significant shear stress, to the top of the canopy. Above the canopy, ν_s first remains close to (or slightly larger than) that at the canopy top and subsequently decreases towards the free surface. This decrease is possibly due to the limited water depth in their flume experiments. They proposed the following scale for the maximum ν_s:

$$\nu_{sm} \propto \Delta U \times t_{ml}, \tag{2.31}$$

where t_{ml} is the thickness of the shear layer, which is defined from $z_1 = h_c - \delta_e$ to a level in the free stream where the shear vanishes, and ΔU is the difference of current velocity

https://doi.org/10.1017/jfm.2022.293 Published online by Cambridge University Press

between the two ends of the shear layer. They also showed that the Reynolds stress at the top of the canopy (see their figure 3) can be related to ΔU via

$$\frac{|\boldsymbol{\tau}_h|}{\rho} = u_{*c}^2 = 0.02\Delta U^2. \tag{2.32}$$

Thus, ΔU in (2.31) can be replaced by the current shear velocity, u_{*c}. Their measurements also showed that t_{ml} is approximately 3 times δ_e (see their table 1), so t_{ml} in (2.31) can be replaced by δ_e. Thus, in this study, the maximum ν_s is

$$\nu_{sm} = c_s u_{*c} \delta_e, \tag{2.33}$$

where c_s is a model parameter to be calibrated. In our model, δ_e is defined as the distance between the canopy top to a level where the mean shear stress is reduced to 5 % of $\boldsymbol{\tau}_h$. As will be shown later, the in-canopy current will be solved by iteration, so δ_e can be evaluated iteratively. Thus, no prior estimate of δ_e is required. Inside the canopy, we simply assume that ν_s linearly decreases from ν_{sm} at $z = h_c$ to 0 at $z = 0$. This simple vertical structure will capture the fact that the canopy-scale shear cannot fully penetrated the whole of the dense canopy. Although the vertical structure can be more complex, it can give satisfactory predictions, so we adopted it in our model.

Immediately above the canopy, it is assumed that the eddy viscosity is depth uniform and takes the value $\nu_T = \nu_{sm}$. At higher levels, the vertical structure of ν_T depends on the water depth above the canopy and the development of overlying flow. For modelling classic open-channel flow, a parabolic eddy viscosity profile is often applied, of which the near-bottom part can be approximated by a linear increase. Studying the eddy viscosity above the canopy would be an interesting research topic, but this is beyond the scope of this study. Here, for simplicity, our model assumes that the canopy is covered by a sufficiently large water depth, so the current velocity profile contains a logarithmic region above the canopy, for which the eddy viscosity linearly increases with the vertical coordinate: $\nu_T = \kappa u_{*c}(z - h_c)$, where κ is the von Kármán constant. This linear eddy viscosity intersects with $\nu_T = \nu_{sm}$ at a transition level

$$\delta_T = \frac{c_s}{\kappa}\delta_e + h_c. \tag{2.34}$$

Note that the parameterization of the above-canopy ν_T does not affect the prediction of the in-canopy current if a current is specified by $\boldsymbol{\tau}_h$ at the top of the canopy and a pressure gradient.

Thus, the whole eddy viscosity profile can be written as

$$\nu_T = \begin{cases} \nu_w + \dfrac{z}{h}\nu_{sm}, & 0 \le z < h_c, \\ \nu_{sm}, & h_c \le z \le \delta_T, \\ \kappa u_{*c}(z - h_c), & T. \end{cases} \tag{2.35}$$

An illustrative sketch of this profile is provided in figure 1. The normalized form of (2.35) is

$$\hat{\nu}_T = \begin{cases} \hat{\nu}_w + \hat{\nu}_{sm}, & \hat{z} < 1, \\ \hat{\nu}_{sm}, & 1 \le \hat{z} \le 1 + \dfrac{c_s}{\kappa}\hat{\delta}_e, \\ \kappa(\hat{z} - 1), & \hat{z} > 1 + \dfrac{c_s}{\kappa}\hat{\delta}_e, \end{cases} \tag{2.36}$$

where

$$\hat{\delta}_e = \frac{\delta_e}{h_c}, \quad \hat{\nu}_w = c_w \frac{(ad)^{4/3}}{\hat{a}} \sqrt{\frac{1}{2}\hat{u}_w^2 + \hat{u}_0^2}, \quad \hat{\nu}_{sm} = c_s \hat{\delta}_e. \tag{2.37a–c}$$

https://doi.org/10.1017/jfm.2022.293 Published online by Cambridge University Press

2.4. *Drag force*

Our model adopts a quadratic drag, i.e. (2.8), for the instantaneous drag force in a wave–current flow. Sarpkaya & Storm (1985) studied the in-line force on a cylinder in collinear wave–current flows. They found that the Morison equation with a quadratic drag force term can nicely fit the measured time series of the in-line force. Some researchers also adopted the same quadratic law in modelling time-varying in-canopy flows (Zeller *et al.* 2015; van Rooijen *et al.* 2020) or analysing experimental results (Hu *et al.* 2014). It should be noted that the nonlinearity of a quadratic law gives a considerable wave–current interaction on the time-averaged drag force, which has been pointed out by some researchers (van Rooijen *et al.* 2020). In fact, the mean drag force can be significantly amplified by a co-existing oscillatory flow, i.e. the drag amplification factor, $\beta_c = \sqrt{\beta_{cx}^2 + \beta_{cy}^2}$, is much larger than 1 (see (2.20) for the definition of β_{ci}). In addition, if wave and current are at an angle of between 0° and 90°, the mean drag force vector and the mean velocity vector may not be in the same direction.

To demonstrate the effect of oscillatory flows on mean drag, a simple illustration is provided here. We first define a wave–current ratio, which is the ratio of the amplitude of oscillatory velocity to the magnitude of current velocity

$$\alpha = \frac{U_w}{|\boldsymbol{u}_c|} = \frac{\hat{u}_w}{|\hat{\boldsymbol{u}}_c|}, \tag{2.38}$$

β_{cx} and β_{cy} can be given by

$$\left.\begin{aligned} \beta_{cx} &= \overline{\sqrt{\alpha^2\cos^2\omega t + 2\alpha\cos\omega t\cos\phi_{wc} + 1}\times(\alpha\cos\omega t + \cos\phi_{wc})}, \\ \beta_{cy} &= \overline{\sqrt{\alpha^2\cos^2\omega t + 2\alpha\cos\omega t\cos\phi_{wc} + 1}\times\sin\phi_{wc}}. \end{aligned}\right\} \tag{2.39}$$

Equation (2.39) shows that both $\beta_c = \sqrt{\beta_{cx}^2 + \beta_{cy}^2}$ and the angle between the drag force and the x-direction, $\phi_d = \tan^{-1}(\beta_{cx}/\beta_{cy})$, are functions of α and ϕ_{wc}. Here, we consider α between 0.1 (an oscillatory flow much weaker than the current) and 10 (an oscillatory flow much stronger than the current). We also choose four angles between wave and current, i.e. $\phi_{wc} = 0°$, 30°, 60° and 90°. Figure 2 presents the variation of β_c and $\phi_d - \phi_{wc}$ with α. For all wave–current angles, β_c is very close to 1 for small values of α, showing that a weak oscillatory flow does not affect the mean drag force. For collinear wave–current flow ($\phi_{wc} = 0°$), β_c increases dramatically as α becomes comparable to or larger than 1, e.g. $\beta_c = 1.49$ for $\alpha = 1$, and 2.64 for $\alpha = 2$. This means a significant increase of mean drag force due to the co-existing oscillatory flow. It is also observed that a larger angle between the wave and current gives a smaller β_c. Note that $\phi_d - \phi_{wc}$ is zero for $\phi_{wc} = 0°$ (the flow is always collinear) and $\phi_{wc} = 90°$ (the oscillatory flow is symmetric). In figure 2(*b*), it can be seen that $\phi_d - \phi_{wc}$ is always negative (or ϕ_d is smaller than ϕ_{wc}), so the mean drag vector veers towards the oscillatory flow. The magnitude of the veering increases with α, and is up to approximately 20° at $\alpha = 10$ and $\phi_{wc} \approx 55°$. For even larger values of α (e.g. $\alpha = 100$), the veering is almost the same as for $\alpha = 10$, so the largest veering angle is approximately 20°. This veering of drag vector will cause veering of the current velocity vector.

Some researchers proposed that the instantaneous drag in wave–current flows can be given as the sum of a mean component and a time-varying component (e.g. Zhou

https://doi.org/10.1017/jfm.2022.293 Published online by Cambridge University Press

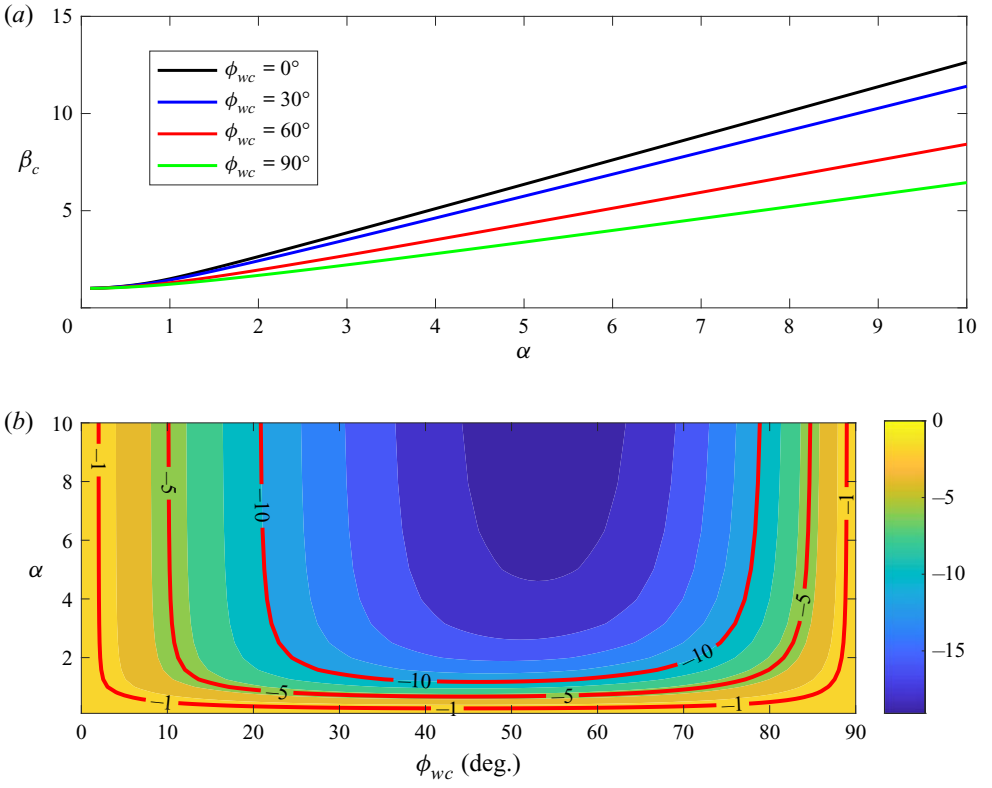


Figure 2. Amplification factor and veering angle of the time-averaged drag force of wave–current in-canopy flows. (*a*) Amplification factor, β_c, (*b*) veering angle, $\phi_d - \phi_{wc}$ (°).

& Graham 2000; Luhar *et al.* 2010). If the drag coefficient of the mean (or current) component is insensitive to the co-existing oscillatory flow, such a decomposition means that the oscillatory flow has little effect on the mean drag experienced by the currents. As will be shown later, our choice of using the quadratic drag can indeed lead to accurate prediction of the current velocity profile, and capture a significant wave effect, so it is more suitable for modelling in-canopy drag.

The drag coefficient in (2.8) and (2.18) is estimated using the model proposed by Ghisalberti & Nepf (2004)

$$C_D(z) = (1 + 10Re_d^{-2/3}) \times \begin{cases} 1.4\left(\dfrac{z}{h_c}\right)^{2.5} + 0.45, & 0 \le z/h_c < 0.76, \\ -4.8\left(\dfrac{z}{h_c}\right) + 4.8, & 0.76 \le z/h_c \le 1, \end{cases} \tag{2.40}$$

where Re_d is a Reynolds number defined based on diameter d. This drag-coefficient model was derived by fitting measurements from unidirectional canopy flow experiments. It accounts for the vertical variation of C_D, which is because the free end of cantilevered cylinder disturbs the wake structure. To account for both the wave and current, Re_d in our application is evaluated using the local r.m.s. velocity

$$Re_d = \frac{\sqrt{0.5U_w^2 + |\boldsymbol{u}_c|^2}d}{\nu}, \tag{2.41}$$

https://doi.org/10.1017/jfm.2022.293 Published online by Cambridge University Press

where ν is the kinematic viscosity of water. The normalized form of (2.40) is

$$C_D(\hat{z}) = \left(1 + 10\left(Re_*\sqrt{\frac{1}{2}\hat{u}_w^2 + |\boldsymbol{u}_c|^2}\right)^{-2/3}\right) \times \begin{cases} 1.4\hat{z}^{2.5} + 0.45, & 0 \le \hat{z} < 0.76, \\ -4.8\hat{z} + 4.8, & 0.76 \le \hat{z} \le 1, \end{cases} \tag{2.42}$$

where

$$Re_* = \frac{u_{*c}d}{\nu}. \tag{2.43}$$

2.5. *Solution of current velocity profile*

The normalized problem is formulated by a normalized governing equation, i.e. (2.21), two boundary conditions, that is (2.22) and (2.23), a closure model for the turbulent eddy viscosity, i.e. (2.36) and (2.37*a–c*), and a closure model for the canopy drag, i.e. (2.18), (2.38), (2.39) and (2.42). A summary of normalization and parameterization is provided in table 2. This system is controlled by the following six dimensionless parameters:

$$Re_*, \quad \hat{u}_w, \quad \hat{S}, \quad \hat{a}, \quad ad, \quad \phi_{\tau h}. \tag{2.44a–f}$$

In dimensional form, the required input parameters are ($\boldsymbol{S}$, U_w, $\boldsymbol{\tau}_h$) for prescribing the flow and (a, h_c, d) for prescribing the canopy.

The normalized problem includes two parameters that must be iteratively determined, i.e. the bottom velocity, ($\hat{u}_{0x}$, $\hat{u}_{0y}$), and the penetration depth $\hat{\delta}_e$. With an initial guess of ($\hat{u}_{0x}$, $\hat{u}_{0y}$) and $\hat{\delta}_e$, the normalized system is solved numerically to give the normalized velocity profile. The numerical scheme is based on the finite volume method and is introduced in Appendix A. The solution is checked to see if it satisfies (2.24), i.e. if the mean shear stress at the canopy top meets the input. If not, ($\hat{u}_{0x}$, $\hat{u}_{0y}$) and $\hat{\delta}_e$ are updated, and a new iteration is conducted. This process continues until the solution converges.

The normalized governing equation of the current outside the canopy is

$$\frac{\partial}{\partial \hat{z}}\left(\hat{\nu}_T \frac{\partial \hat{u}_{ci}}{\partial \hat{z}}\right) = -\hat{S}_i. \tag{2.45}$$

Integrating this equation from the top of the canopy ($\hat{z} = 1$) to $\hat{z}$ gives

$$\hat{\nu}_T \frac{\partial \hat{u}_{ci}}{\partial \hat{z}} = -\hat{S}_i(\hat{z} - 1) + \hat{\tau}_{hi}, \quad i = x, y. \tag{2.46}$$

Using the profile of the normalized eddy viscosity, this equation can be integrated upward from $\hat{z} = 1$, where the current velocity is obtained by numerically solving the in-canopy flow. The analytical solution of the above-canopy current is

$$\hat{u}_{ci} = \begin{cases} \hat{u}_{hi} + \dfrac{\hat{\tau}_{hi} + \hat{S}_i}{c_s\hat{\delta}_e}(\hat{z} - 1) - \dfrac{\hat{S}_i}{2c_s\hat{\delta}_e}(\hat{z}^2 - 1), & 1 < \hat{z} \le 1 + \dfrac{c_s}{\kappa}\hat{\delta}_e, \\ \dfrac{\hat{\tau}_{hi}}{\kappa}\ln\left(\dfrac{\hat{z} - 1}{\hat{z}_{0a,i}}\right) - \dfrac{\hat{S}_i}{\kappa}(\hat{z} - 1), & \hat{z} > 1 + \dfrac{c_s}{\kappa}\hat{\delta}_e \end{cases}, \tag{2.47}$$

where the apparent roughness is given by

$$\hat{z}_{0a,i} = \frac{c_s\hat{\delta}_e}{\kappa}\exp^{-1}\left(\frac{\kappa\hat{u}_{hi}}{\hat{\tau}_{hi}} + 1 + \frac{c_s\hat{\delta}_e}{2\kappa\hat{\tau}_{hi}}\hat{S}_i\right). \tag{2.48}$$

https://doi.org/10.1017/jfm.2022.293 Published online by Cambridge University Press

Item	Remarks
Non-dimensional variables	
$\widehat{\boldsymbol{u}_c} = (\hat{u}_{cx}, \hat{u}_{cy}) = \left(\dfrac{u_{cx}}{u_{*c}}, \dfrac{u_{cy}}{u_{*c}}\right)$	Current velocity
$\hat{u}_w = U_w/u_{*c}$	Wave velocity
$\hat{\nu}_T = \nu_T/(u_{*c}h_c)$	Turbulent eddy viscosity
$\hat{z} = z/h_c$	Vertical coordinate
$\hat{\boldsymbol{S}} = (\hat{S}_x, \hat{S}_y) = \left(\dfrac{gh_cS_x}{u_{*c}^2}, \dfrac{gh_cS_y}{u_{*c}^2}\right)$	Mean pressure gradient
$(\hat{f}_{dx}, \hat{f}_{dy}) = \dfrac{(f_{dx}, f_{dy})}{u_{*c}^2/h_c}$	Canopy drag
$\hat{a} = ah_c$	Solidity
$\varphi_{\tau h}$	Angle between $\boldsymbol{\tau}_h$ and the x-direction
Governing equations and boundary conditions	
$\left.\begin{aligned}\dfrac{\partial}{\partial\hat{z}}(\hat{\nu}_T\dfrac{\partial\hat{u}_{cx}}{\partial\hat{z}}) &= -\hat{S}_x + \hat{f}_{dx},\\ \dfrac{\partial}{\partial\hat{z}}(\hat{\nu}_T\dfrac{\partial\hat{u}_{cy}}{\partial\hat{z}}) &= -\hat{S}_y + \hat{f}_{dy},\end{aligned}\right\}$	Governing equation
$\hat{\boldsymbol{u}}_c = (\hat{\boldsymbol{u}}_{0x}, \hat{\boldsymbol{u}}_{0y}) = \left(\dfrac{u_{0x}}{u_{*c}}, \dfrac{u_{0y}}{u_{*c}}\right), @\hat{z} = 0$	Slip bottom boundary condition
$\dfrac{\partial\hat{u}_{ci}}{\partial\hat{z}} = 0, \quad \text{at } \hat{z} = 0,\ i = x, y$	Zero-gradient bottom boundary condition
$\left(\hat{\nu}_T\dfrac{\partial\hat{u}_{cx}}{\partial\hat{z}},\ \hat{\nu}_T\dfrac{\partial\hat{u}_{cy}}{\partial\hat{z}}\right) = (\cos\phi_{\tau h}, \sin\phi_{\tau h}), @\hat{z} = 1$	Model restriction
Canopy drag	
$(\hat{f}_{dx}, \hat{f}_{dy}) = \dfrac{1}{2}C_D\hat{a}\hat{u}_c^2(\beta_{cx}, \beta_{cy})$	Quadratic drag
$(\beta_{cx}, \beta_{cy}) = \dfrac{\lvert\hat{\boldsymbol{u}}(z,t)\rvert\hat{\boldsymbol{u}}(z,t)}{\hat{u}_c^2}$	Drag amplification factor
$C_D(\hat{z}) = (1 + 10(Re_*\sqrt{\dfrac{1}{2}\hat{u}_w^2 + \lvert\boldsymbol{u}_c\rvert^2})^{-2/3}) \times \begin{cases}1.4\hat{z}^{2.5} + 0.45, & 0 \le \hat{z} < 0.76\\ -4.8\hat{z} + 4.8, & 0.76 \le \hat{z} \le 1\end{cases}$	The C_D from Ghisalberti & Nepf (2004). $Re_* = u_{*c}d/\nu$
Turbulent eddy viscosity	
$\hat{\nu}_T = \begin{cases}\hat{\nu}_w + \hat{\nu}_{sm}, & \hat{z} < 1\\ \hat{\nu}_{sm}, & 1 \le \hat{z} \le 1 + \dfrac{c_s}{\kappa}\hat{\delta}_e\\ \kappa(\hat{z} - 1), & \hat{z} > 1 + \dfrac{c_s}{\kappa}\hat{\delta}_e\end{cases}$	Two components inside canopy Constant-linear structure above canopy
$\hat{\nu}_w = c_w\dfrac{(ad)^{4/3}}{\hat{a}}\sqrt{\dfrac{1}{2}\hat{u}_w^2 + \hat{u}_0^2}$	Wake-related component, $c_w = 0.024$, combined Tanino & Nepf (2008*b*); King *et al.* (2012), Zhang *et al.* (2018).
$\hat{\nu}_{sm} = c_s\hat{\delta}_e$	Shear-related eddy viscosity at canopy top, based on Ghisalberti & Nepf (2004) $\hat{\delta}_e = \delta_e/h_c$: a penetration length scale c_s is given by (3.2)

Table 2. Summary of the proposed model, including normalization, governing equations, boundary conditions and parameterizations.

https://doi.org/10.1017/jfm.2022.293 Published online by Cambridge University Press

Test ID	Reference	ah_c	ad	$h/h_c - 1$	c_s	ϵ_L	ϵ
Test 5b	Chen *et al.* (2020)	0.402	0.011	1.3	0.09	18.8 %	6.2 %
Test 5c	Chen *et al.* (2020)	0.798	0.021	1.3	0.13	−3.7 %	−6.1 %
Test S5B	King *et al.* (2012)	0.772	0.012	0.9	0.14	2.4 %	−7.0 %
Test S6C	King *et al.* (2012)	0.776	0.025	0.9	0.10	15.9 %	8.0 %
Test H	Ghisalberti & Nepf (2004)	1.104	0.051	2.4	0.61	−10.3 %	−2.1 %
Test C	Ghisalberti & Nepf (2004)	0.469	0.022	2.4	0.65	−11.1 %	−6.0 %
Test U5	Lowe *et al.* (2005)	0.500	0.250	3.3	0.39	−3.3 %	9.3 %
Test U7	Lowe *et al.* (2005)	0.222	0.111	3.3	0.50	−1.6 %	2.1 %

Table 3. Unidirectional flume tests used for model calibration.

3. Model calibration and validation

3.1. *Model calibration*

The parameter, c_s, in the shear-related eddy viscosity, i.e. (2.33), requires calibration. We chose the measurements from four groups of unidirectional flume experiments, which used an array of cylinders as the canopy, for the model calibration. Three dimensionless parameters, $\hat{a}$, ad, $h/h_c - 1$, of the canopies in these tests are provided in table 3. The solidity $\hat{a}$ is from 0.22 to 1.1, so all canopies can be considered as dense canopies ($\hat{a} > 0.1$, cf. Nepf 2012). The parameter, ad, which represents the solid volume fraction, is from 0.01 to 0.2. The submergence, $h/h_c - 1$, is between 0.9 and 3.3, which is applicable for typical submerged aquatic canopies.

Our model is driven by the mean shear stress at the canopy top and the mean pressure gradient of the open channel. These two parameters can only be estimated from the velocity measurements. In view of this, an iteration scheme is proposed to apply our model. The current is specified by a reference current velocity at a reference level slightly above the canopy, and there is reason for doing so. Note that the submergence of some tests is not very large (e.g. the water depth is only approximately twice of the canopy height). For these tests, our simple linearly increasing eddy viscosity above the canopy may not work. By having a reference velocity very close to the canopy top, the prediction of in-canopy flow will not be affected by the inadequacy of modelling above-canopy flow. The normalized mean pressure gradient is estimated following (2.6), i.e.

$$\hat{S} = \frac{h_c}{h - h_c}. \tag{3.1}$$

The value of the shear velocity, u_{*c}, is iteratively updated, until the model gives the reference current velocity. This iterative scheme was also applied to the wave–current tests in the next subsection.

The optimal value of c_s, which gives the best model–data agreement for the in-canopy current velocity, was obtained for each test in the calibration, and the results are provided in table 3. Here, the agreement is evaluated using the averaged r.m.s. error. It appears that the tests can be divided into two groups. The first group includes the first four rows of table 3, which have c_s between 0.09 and 0.14. The second group includes the last four rows of table 3, which have c_s between 0.39 and 0.65. By checking the values of $\hat{a}$, ad and $h/h_c - 1$, it seems that c_s is correlated with the submergence $h/h_c - 1$. In the first group, $h/h_c - 1$ is close to 1, so the thickness of water above the canopy is approximately the same as the canopy height. In the second group, $h/h_c - 1$ is between 2.4 and 3.3, meaning

https://doi.org/10.1017/jfm.2022.293 Published online by Cambridge University Press

that the thickness of water above the canopy is approximately 2.4 to 3.3 times the canopy height.

The shear-related eddy viscosity characterizes the mixing of momentum due to the canopy-scale KH vortex in the upper part of the canopy. In fact, the characteristics of the KH vortices are controlled by the submergence of the canopy. For instance, Ghisalberti & Nepf (2002) showed that the translation velocity of KH vortices increases with the submergence of the canopy. Thus, it can be argued that the shear-related eddy viscosity is also affected by the submergence. The size of the KH vortex is comparable to h_c, so it is possible that the limited water depth above the canopy affects the development or the behaviour of KH vortices, if $h/h_c - 1$ is close to or smaller than 1. Accurately quantifying c_s as a function of $h/h_c - 1$ requires a large set of experiments, especially for the tests with $h/h_c - 1$ between 1.3 and 2.4. Since the focus of this study is on wave–current interaction within the canopy, we shall leave this for the future. Here, we simply adopt a three-leg structure that gives an increasing c_s between $(h/h_c - 1) = 1.3$ and 2.4

$$c_s = \begin{cases} 0.12, & h/h_c - 1 < 1.3, \\ 0.3818(h/h_c - 1) - 0.3764, & 1.3 \le h/h_c - 1 < 2.4, \\ 0.54, & h/h_c - 1 \ge 2.4. \end{cases} \tag{3.2}$$

For very low submergence, large-scale flow structure (here the KH vortex) will lead to undulation of the free surface, or the propagating wave's trough may touch the canopy. In such cases, the free surface dynamics may also control the vertical momentum transfer in the upper canopy. We leave the investigation of very low submergence to the future.

Figure 3 presents the model–data comparisons for the eight tests in the calibration. To quantify the error, we introduced an error index

$$\epsilon = \frac{\sum prediction - \sum measurement}{\sum measurement}. \tag{3.3}$$

This index measures the relative error in predicting the overall flow rate. Two error values were evaluated. The first one, ϵ, was calculated using all measured data points below the canopy top ($0 \le \hat{z} < 1$), so it indicates the overall model performance for in-canopy current. The second one, ϵ_L, was calculated using the data points below the penetration depth ($0 \le \hat{z} < 1 - \hat{\delta}_e$), so it shows the model error for the lower part of the canopy. The results are presented in the last two columns of table 3.

The model captures the vertical variation of current inside the canopy ($0 \le \hat{z} < 1$). A nearly depth-invariant current is predicted in the lower part of the canopy for the four shallow-submergence tests with $c_s = 0.12$. For the four deep-submergence tests with $c_s = 0.54$, the shear (vertical gradient of current velocity) is visible in the lower part of the canopy, but the magnitude is much lower than that near the top of the canopy. The shape of the profile, which is characterized by an infection point around the top of the canopy ($\hat{z} = 1$), is well produced by the model. There are some discrepancies in the above-canopy region, indicating that the proposed eddy viscosity above the canopy can be further refined for describing the shear layer above the canopy. The error, ϵ_L, of the lower layer is generally around 10 %, while the error, ϵ, of the whole canopy is below 10 %.

3.2. *Model validation*

In this section, the model is applied to predict the in-canopy current for wave–current flows through a submerged dense canopy. The recent flume study by Chen *et al.* (2020) are used for model validation. In this study, co-directional wave–current flows were

https://doi.org/10.1017/jfm.2022.293 Published online by Cambridge University Press

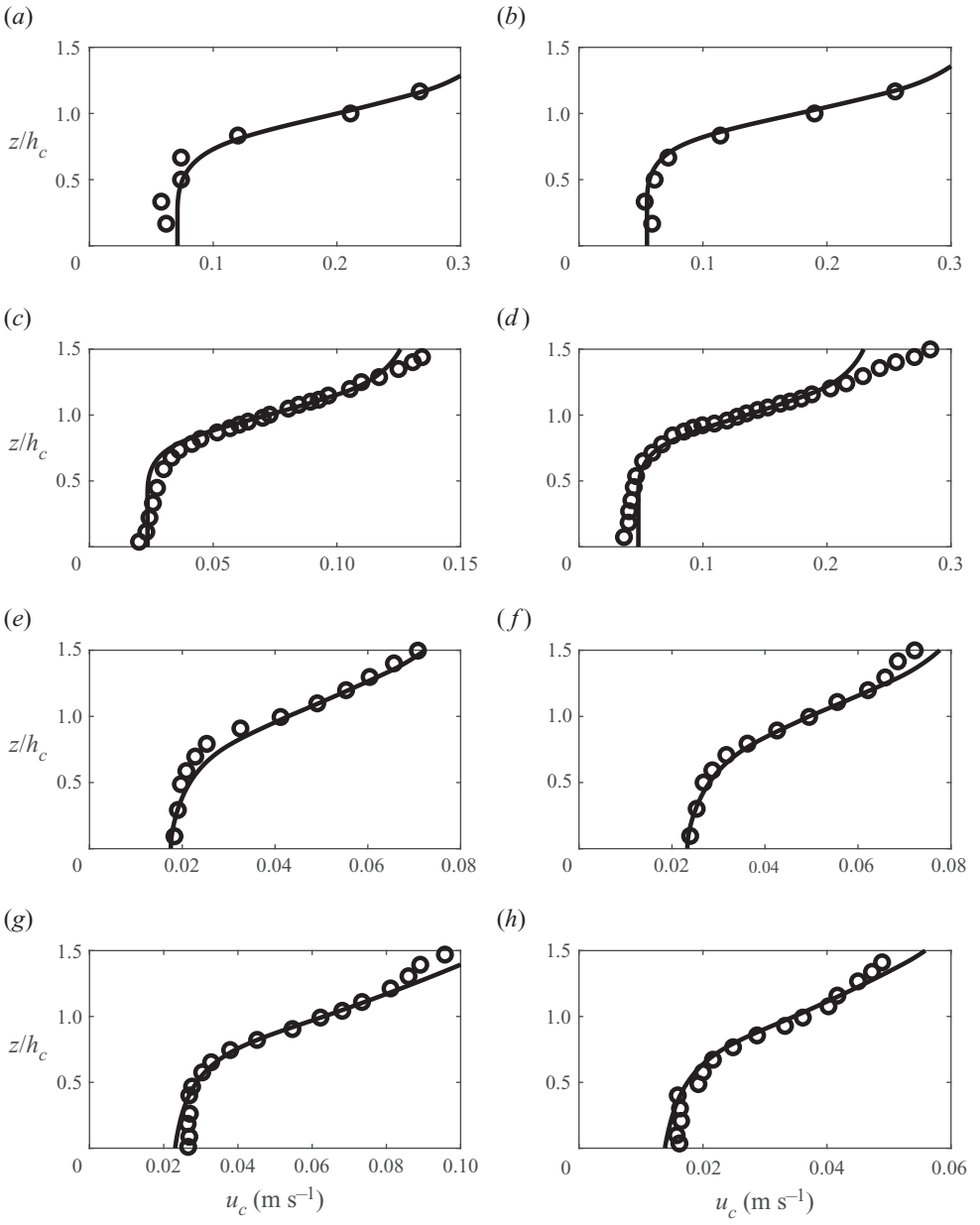


Figure 3. Prediction of in-canopy current profile for pure-current flume tests (circles, measurements; solid lines, predictions; see table 3 for test conditions). (*a*) Test 5b, $c_s = 0.12$. (*b*) Test 5c, $c_s = 0.12$. (*c*) Test S5B, $c_s = 0.12$. (*d*) Test S6C, $c_s = 0.12$. (*e*) Test U5, $c_s = 0.54$. (*f*) Test U7, $c_s = 0.54$. (*g*) Test H, $c_s = 0.54$. (*h*) Test C, $c_s = 0.54$.

generated in a 50 m long, 1.2 m wide and 0.8 m deep flume. A 6 m long vegetated zone was installed in the middle of the flume. The submerged canopy was an array of unstaggered cylinders ($d = 8$ mm). We choose the two canopy configurations (*b*,*c*), which have uniform vegetation density throughout the entire canopy, for our model validation. The canopy height was 0 cm, while the water depth was 0.7 m. For each canopy configuration, there

https://doi.org/10.1017/jfm.2022.293 Published online by Cambridge University Press

Test ID	U_w(m s^{-1})	u_{cr}^a (m s^{-1})	a (m^{-1})	u_{*c} (m s^{-1})	$\hat{u}_w$	$\hat{\tau}_w$	ϵ_L	ϵ
6b	0.073	0.266	1.34	0.027	2.7	2.1 %	4.0 %	4.7 %
6c	0.069	0.260	2.66	0.032	2.2	2.4 %	−6.7 %	8.0 %
7b	0.098	0.286	1.34	0.029	3.3	4.1 %	14.9 %	−0.5 %
7c	0.097	0.234	2.66	0.031	3.1	7.3 %	−14.9 %	−0.8 %
8b	0.114	0.294	1.34	0.031	3.7	5.9 %	53.0 %	8.3 %
8c	0.115	0.265	2.66	0.035	3.3	9.3 %	4.3 %	28.3 %
9b	0.143	0.300	1.34	0.033	4.4	10.4 %	41.9 %	−2.9 %
9c	0.138	0.255	2.66	0.036	3.9	15.7 %	15.2 %	5.2 %

Table 4. Input parameters and key output parameters of the wave–current tests of Chen *et al.* (2020).

[a]The reference level is $z = 35$ cm.

were four wave–current tests (named as Test 6 to Test 9). In these tests, the waves have the same period (1.8 s) and wave heights increased from 6 cm (Test 6) to 12 cm (Test 9). The current was specified by the total flow rate in the flume, and the 'same' current of a 140 s^{-1} flow rate was produced in all tests, which means the cross-section-averaged current velocity was approximately 17 cm s^{-1}. The flow velocity was sampled at a 5 cm vertical interval using an acoustic Doppler velocimetry (ADV) installed in the void among the cylinders. The ADV measurements showed that the oscillatory flow inside the canopy was approximately $10 \sim 20$ cm s^{-1}, and was quite depth uniform. The in-canopy current had the typical vertical profile of the in-canopy unidirectional flow, and the current magnitude was generally below 10 cm s^{-1} (see their figure 5).

The input parameters are determined as follows. The amplitude of the oscillatory flow measured at 10 cm from the bottom (or 20 cm below the canopy top) was taken as the amplitude of the in-canopy oscillatory flow, U_w. The current is specified by a reference current velocity, u_{cr}, measured at 5 cm above the canopy (or 35 cm from the bottom). The canopy is described by $d = 8$ mm, $h_c = 30$ cm, $h = 70$ cm and the front area per unit volume, α. Table 4 summarizes the values of U_w, u_{cr} and α, for all tests involved in the model validation.

The comparisons between measurements and predictions are shown in figure 4, and the quantification of model error is provided in the last two columns of table 4. Overall, the model–data agreement is similar to the pure-current cases in figure 3. The current profile in the upper part of the canopy, where a strong vertical gradient is present, is well predicted by the model. This suggests that the simple eddy viscosity model, which is calibrated using only pure-current flows, works for these wave–current flume tests. Using the predicted shear velocity, u_{*c}, it is found that the normalized wave velocity, $\hat{u}_w = U_w/u_{*c}$ is generally between 2 and 4. Thus, it can be speculated that an in-canopy oscillatory flow with $\hat{u}_w < 4$ has insignificant effect on the current-generated KH vortices at the canopy top. The model also predicts a weak in-canopy flow with little vertical gradient in the lower part of the canopy. For c-group tests (denser canopy, the right column of figure 4), both the prediction and the measurement have a quite depth-uniform flow near the bottom of the canopy. For some b-group tests (sparser canopy, see Tests 8b and 9b), the measured velocity profile seems to have some vertical gradient near the bottom. Using (2.1) and simply $C_D = 1$, the penetration depth for b-group tests ($a = 1.34$ m^{-1}) is found to be 17 cm, which is approximately half of the canopy height. Thus, the canopy should be sufficiently dense to give a lower in-canopy layer, where the drag force is mostly balanced by the pressure gradient. As shown in figure 5(*a*), the unidirectional flow test (Test 5b) of

https://doi.org/10.1017/jfm.2022.293 Published online by Cambridge University Press

the same canopy indeed has a quite depth-uniform lower layer in the current profile. One possible explanation of the observed near-bottom velocity gradient is the spatial variation of drag coefficient. A uniform in-canopy flow requires a constant drag coefficient and a balance between mean drag and pressure gradient. In wave–current flows, the mean drag is influenced by the drag amplification factor, β_c, defined in (2.20). Note that β_c is partly influenced by the amplitude of oscillatory flow. In the very vicinity of the bottom, the oscillatory flow should have some vertical variation, since it must be reduced to zero at the bottom to meet the no-slip boundary condition. This will lead to a strong vertical variation of β_c, which cannot be captured by our model, due to the assumption of a depth-uniform oscillatory flow. The error, ϵ_L, of the lower layer indeed increases with the wave condition (wave amplitude increases from Test 6b to 9b), but except for Tests 8b and 9b, ϵ_L is approximately 10 %, which is comparable to that of the calibration tests. The overall error of the whole layer, except for one test (Test 8c), is also below 10 %. Thus, the model performance for the validation tests is similar to that for the calibration tests.

To show more details of our model, here the predictions of the mean canopy drag, Reynolds stress and drag amplification factor of a representative test, Test 9c, are presented in figure 5. To highlight the effect of waves, a corresponding pure-current prediction was conducted by setting the oscillatory velocity to zero. The results are also provided in figure 5 for comparison. From figure 5(*a*), it can be seen that adding an oscillatory flow significantly reduces the in-canopy current velocity by roughly a factor of 2. The driving force of the current, i.e. the pressure gradient and the shear stress at the canopy top (see figure 5*c*), in the wave–current prediction is only approximately 30 % larger than that in the pure-current prediction. Accordingly, the mean canopy drag of the wave–current prediction is approximately 30 % to 50 % larger than that of the pure-current prediction (see figure 5*b*). The drag amplification factor, β_c, of the wave–current prediction, however, is up to 6.5 inside the canopy (see figure 5*d*), since the ratio of wave velocity to current velocity is approximately 5 inside the canopy. Thus, the current velocity of the wave–current prediction must be 50 % smaller than that of the pure-current prediction, in order to give the required mean drag. This comparison demonstrates that the nonlinear wave–current interaction originating from the quadratic drag law indeed can have a pronounced effect on in-canopy current. More in-depth discussions will be provided in the next section.

The potential contribution of wave-induced mean canopy flow to wave–current interaction is worth some discussion. According to Luhar *et al.* (2010), waves pump momentum and energy into a submerged canopy, which leads to an in-canopy mean flow. Assuming that the energy dissipation due to canopy drag balances the wave-induced energy influx, the wave-induced momentum influx or a mean wave stress at the top of the canopy can be written as

$$\frac{\tau_w}{\rho} = (-\overline{uw})_{w,top} = \dot{E}/c, \tag{3.4}$$

where $\dot{E}$ is the energy dissipation rate within the canopy, and c is the wave celerity. Assume depth-uniform oscillatory flow and a quadratic drag law

$$\dot{E} = \int_0^{h_c} U_w F_D \,\mathrm{d}z = \frac{2}{3\pi}\rho C_D a h_c U_w^3. \tag{3.5}$$

Substitute (3.5) into (3.4), the wave stress at canopy top is

$$\frac{\tau_w}{\rho} = \frac{2}{3\pi}\rho a C_D \left(\frac{U_w}{c}\right) U_w^2 h_c. \tag{3.6}$$

https://doi.org/10.1017/jfm.2022.293 Published online by Cambridge University Press

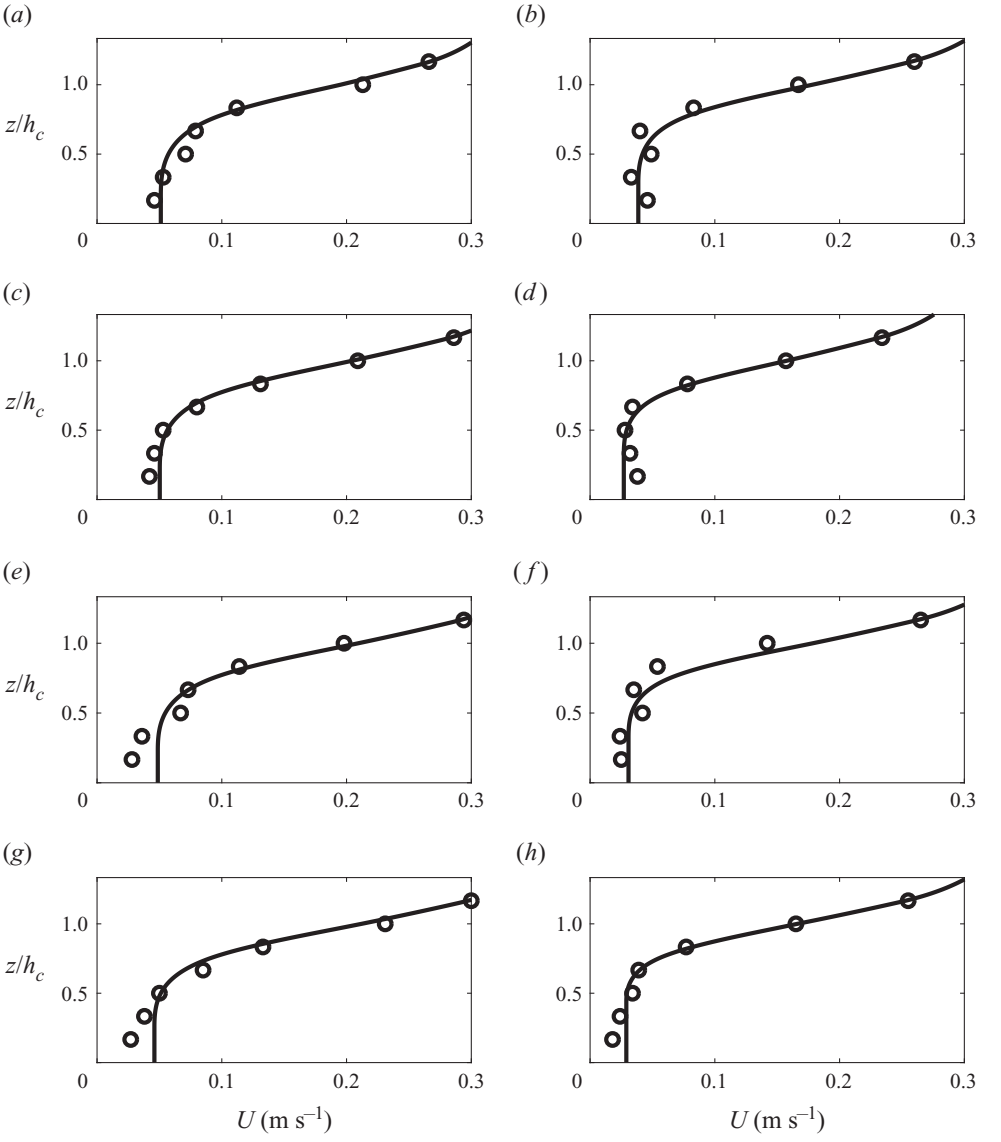


Figure 4. Model validation for current velocity profiles in wave–current canopy flows (circles, measurements; solid lines, predictions). (*a*) Test 6b. (*b*) Test 6c. (*c*) Test 7b. (*d*) Test 7c. (*e*) Test 8b. (*f*) Test 8c. (*g*) Test 9b. (*h*) Test 9c.

The relative importance of the wave-induced mean in-canopy flow can be assessed by the ratio of τ_w to τ_h, i.e.

$$\hat{\tau}_w = \frac{\tau_w}{\tau_h} = \frac{2}{3\pi}\hat{a}C_D\left(\frac{U_w}{c}\right)\hat{u}_w^2. \tag{3.7}$$

Based on (3.7), the contribution of wave-induced mean flow increases with the solidity of the canopy ($\hat{a}$), the relative strength of the wave ($\hat{u}_w$), but decreases with wave celerity. Using wave celerity estimated by linear wave theory, $\hat{\tau}_w$ of the eight validation tests is evaluated and presented in the last column of table 4. The highest $\hat{\tau}_w$ (15.7 %) is from Test 9c, since this test has the highest value of U_w/c, and the larger $\hat{a}$. For most of the tests,

https://doi.org/10.1017/jfm.2022.293 Published online by Cambridge University Press

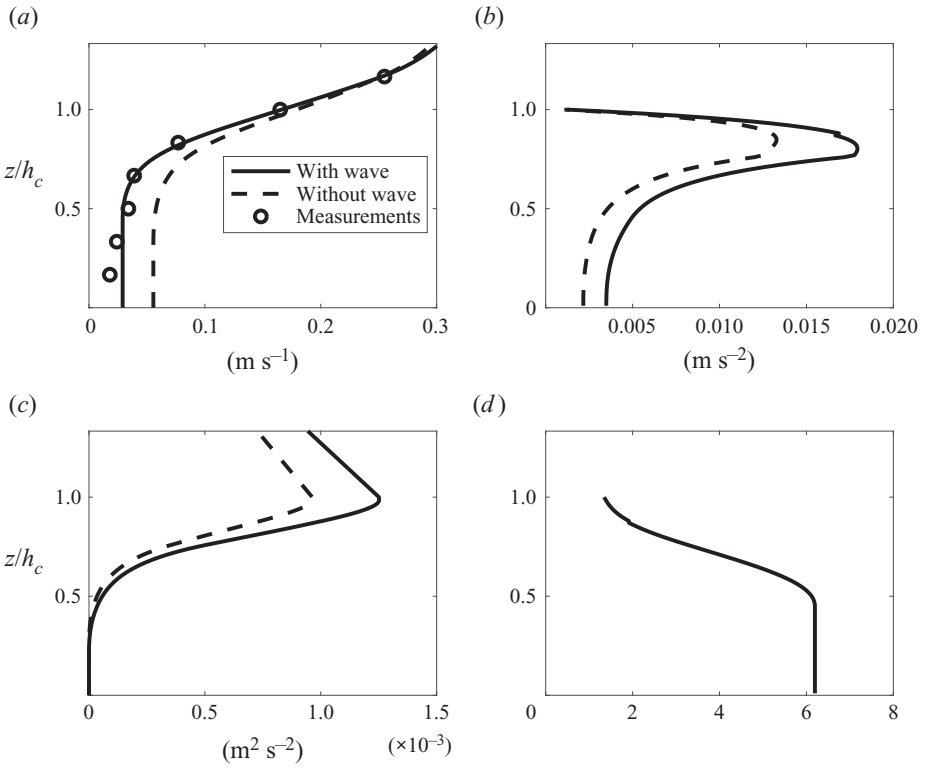


Figure 5. Prediction of Test 9c (the top of the canopy is at $z = 0.3$ m): (*a*) current velocity u_c, (*b*) drag force f_d, (*c*) Reynolds shear stress τ/ρ, (*d*) drag amplification factor β_c.

$\hat{\tau}_w$ is less than 10 %, so the mean wave stress is much smaller than the mean shear stress at the canopy top. Therefore, it is reasonable to neglect wave-induced mean canopy flow in these tests. In shallow coastal regions, the ratio U_w/c is usually around or less than 0.1 (e.g. 1 m high wave with a 4 s wave period gives $U_w/c = 0.14$ for a water depth of 3 m). Assuming C_D is around $1 \sim 2$, a wave-induced mean flow is not important if $2\hat{a}\hat{u}_w^2/3\pi$ is of $O(1)$.

4. Effects of oscillatory flows on in-canopy current

In this section, the effect of wave-induced oscillatory flow on in-canopy current is discussed in a more systematic manner. Based on the normalization of the governing equation and closure models in § 2, the system is controlled by five non-dimensional parameters ($\hat{a}$, ad, Re_*, $\hat{u}_w$ and $\hat{S}$) and the angle between wave and current. We shall focus on typical submerged coastal canopies, e.g. seagrass meadows or coral communities, for which the solid volume fraction is low. The representative values of these parameters to be used in this section are listed as follows:

(i) $ad = 0.02$. This parameter is proportional to the solid volume fraction. Typical seagrass meadows or coral canopies have a solid volume fraction of $O(0.01)$. In our model, ad controls the wake-related eddy viscosity, which does not play a significant role in determining the in-canopy current, so we simply take a single value, $ad = 0.02$, in the following analysis.

https://doi.org/10.1017/jfm.2022.293 Published online by Cambridge University Press

(ii) $\hat{a} = [0.5, 1, 5]$. This parameter is solidity or the front area per bed area. For branched reef corals, Lowe *et al.* (2005) summarized the values of $\hat{a}$ of several studies and showed that $\hat{a}$ is generally between 0.5 and 2. For seagrass meadows, a summary of typical $\hat{a}$ values provided by Luhar *et al.* (2010) showed that $\hat{a}$ is normally between 1 and 15. The influence of $\hat{a}$ will be studied by comparing the predictions using $\hat{a} = 0.5$, 1 and 5.

(iii) $Re_* = 500$. The Reynolds number mainly affects the prediction of canopy drag coefficient. For typical aquatic canopies, the representative stem diameter, d, is around 1 cm. As a rule of thumb estimate, the current shear velocity, u_{*c}, is one order of magnitude smaller than the current velocity at the edge of the canopy, so the typical value of u_{*c} should be in the range $1 \sim 10\,\mathrm{cm\,s^{-1}}$ (assuming a current velocity at the canopy top from $10\,\mathrm{cm\,s^{-1}}$ to $1\,\mathrm{m\,s^{-1}}$). Thus, Re_* is expected to be between 100 and 1000. Sensitivity analysis shows that the prediction is not very sensitive to the variation of Re_* within 100 to 1000. Here, we simply take a single value $Re_* = 500$.

(iv) $|\hat{\boldsymbol{S}}| = [1, 1/3]$. For fully developed flow in open channels, the magnitude of the normalized pressure gradient is related to the submergence of the canopy, i.e. (3.1). For coastal flows, (3.1) is not necessarily valid, but can still be used to assess the relative importance of the pressure gradient. It is assumed that the pressure gradient and the shear stress at the canopy top are in the same direction. Here, we consider two typical submergence values for aquatic canopies submerged in shallow coastal regions, $|\hat{\boldsymbol{S}}| = [1, 1/3]$, i.e. the water depth is 2 or 4 times the height of the canopy (hereafter referred to as the shallow and deep submergences). Having only two levels of $|\hat{\boldsymbol{S}}|$ is also because our model parameter, c_s, is found to vary with $|\hat{\boldsymbol{S}}|$, but the variation is not well modelled at present.

(v) $\hat{u}_w$ between 0 and 5. This parameter is the one that directly characterizes the waves' effect on current. As discussed in the previous section, a very large $\hat{u}_w$ may give a strong wave-induced in-canopy flow, which is not included in the present model, so here we limit the range of $\hat{u}_w$ to [0, 5] ($\hat{u}_w = 0$ means a pure-current condition). Note that the adopted $Re_* = 500$ is associated with a u_{*c} between 1 and $10\,\mathrm{cm\,s^{-1}}$, so $\hat{u}_w$ in [0, 5] represents an oscillatory flow up to $50\,\mathrm{cm\,s^{-1}}$. It is unusual to have an in-canopy oscillatory flow that far exceeds $50\,\mathrm{cm\,s^{-1}}$, since such strong flows may cause severe damage to the canopy organisms. Thus, having $\hat{u}_w \sim [0, 5]$ is realistic.

Based on these discussions, we are able to reduce the dimension of the parameter study. By fixing the values for ad and Re_* and having discrete values for $|\hat{\boldsymbol{S}}|$ and $\hat{a}$, the wave–current interaction under a given $\phi_{\tau h}$ only depends $\hat{u}_w$, which can be easily presented in a graph.

The most significant effect of oscillatory flow is the retardation of in-canopy flow. The veering of in-canopy current, which is due to a finite angle between waves and currents, will also be investigated in § 4.2.

4.1. *Collinear wave–current flow*

An oscillatory flow inside the canopy amplifies the mean canopy drag force experienced by the current. Under the same driving force, the in-canopy current of a wave–current flow can be significantly reduced from that of a unidirectional flow. This effect can be illustrated by comparing a series of collinear wave–current predictions with varying values of $\hat{u}_w$. Figure 6 compares three predictions with the same submergence ($S = 1$), canopy

https://doi.org/10.1017/jfm.2022.293 Published online by Cambridge University Press

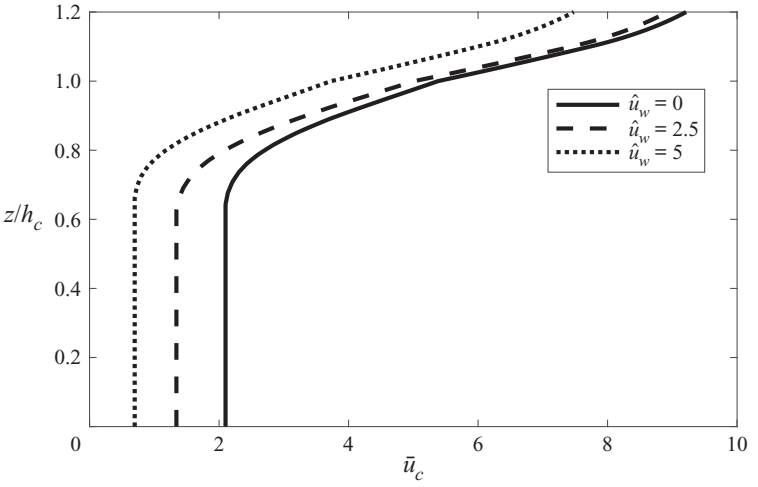


Figure 6. Normalized current velocity profile for a shallow-submergence canopy ($\hat{S} = 1$, $ad = 0.02$, $\hat{a} = 1$, $Re_* = 500$).

density ($\hat{a} = 1$) but different wave strengths ($\hat{u}_w = 0$, 2.5 and 5). It can be clearly seen that the current velocity reduces significantly with increasing $\hat{u}_w$, In the near-bottom region, the current under $\hat{u}_w = 5$ is less than half of that without a wave ($\hat{u}_w = 0$). The reduction reduces towards the top of the canopy, i.e. at $z/h_c = 1$ the current under $\hat{u}_w = 5$ is only approximately 17 % smaller than that without a wave. Therefore, it can be concluded that the wave's effect is more important in the lower part of the canopy.

To give an overall picture of wave-related reduction of in-canopy current velocity, the depth-averaged in-canopy current velocity, $\hat{u}_{ca}$, is considered. For given values of Re_*, ad, $\hat{a}$ and $\hat{S}$, $\hat{u}_{ca}$ is a function of $\hat{u}_w$. We calculated $\hat{u}_{ca}$ for $\hat{u}_w$ between 0 and 5, and evaluated the ratio $r_u = \hat{u}_{ca}/\hat{u}_{ca,0}$, where $\hat{u}_{ca,0}$ is from the pure-current prediction. Here, r_u quantifies the overall reduction of in-canopy current. The results for the two submergence (shallow, $\hat{S} = 1$, and deep $\hat{S} = 1/3$) and three canopy solidities ($\hat{a} = 0.5, 1, 5$) are presented in figure 7. It can be easily seen that more reduction of current occurs for a denser canopy and stronger wave condition, while the effect of submergence is insignificant. For a sparse canopy ($\hat{a} = 0.5$), the reduction is approximately 10 % ($r_u = 0.9$) under $\hat{u}_w \approx 2$, and is increased to approximately 50 % under $\hat{u}_w \approx 5$. For a dense canopy ($\hat{a} = 5$), a 10 % reduction can be achieved for $\hat{u}_w < 1$, and $\hat{u}_w = 5$ can give $80 \sim 90$ % reduction of $\hat{u}_{ca}$. Under the same driving force, a denser canopy has a smaller in-canopy current, which gives a larger wave–current ratio, $\alpha = U_w/u_c$. The drag amplification factor increases with α, so a dense canopy has more reduction of the in-canopy current velocity in order to maintain a drag force similar to that in a sparse canopy.

4.2. *Wave and current at an angle*

As shown in figure 2, when the wave and current inside the canopy are at an angle between 0 ° and 90 °, the drag force vector is not aligned with the current velocity vector, but veers towards the waves. For a fully developed in-canopy current, if the two driving forces of in-canopy current, i.e. the mean shear stress at the canopy top and the mean pressure gradient, are in the same direction, the total drag force (vertical integral of canopy drag) must balance the sum of the two driving forces. Therefore, for pure-current flow, the

https://doi.org/10.1017/jfm.2022.293 Published online by Cambridge University Press

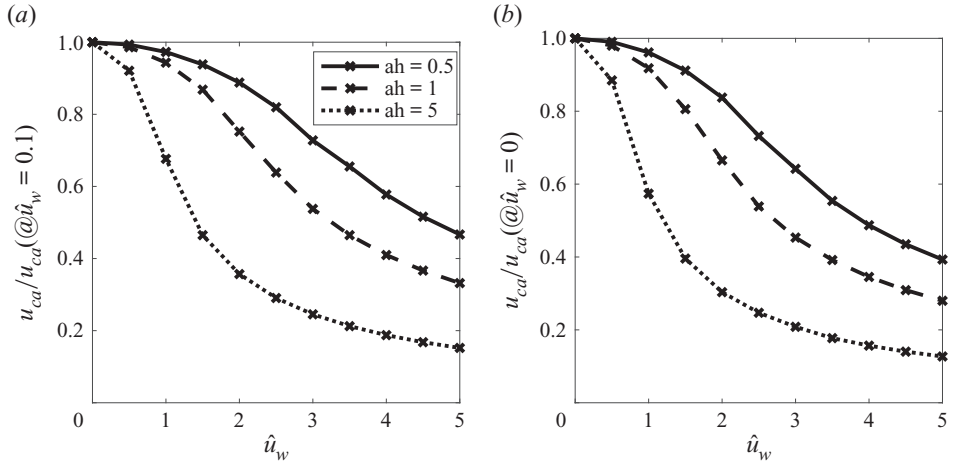


Figure 7. The variation of depth-averaged in-canopy flow with the relative wave strength $\hat{u}_w$: (*a*) shallow submergence, average in-canopy velocity, $\hat{S} = 1$, $c_s = 0.12$; (*b*) deep submergence, average in-canopy velocity, $\hat{S} = 1/3$, $c_s = 0.54$.

current velocity vector must be aligned with the driving force vectors. For wave–current flows, however, the current velocity vector should veer away from the driving force vectors (here 'away' means enlarging the angle between the current velocity vector and the axis of the oscillatory flow) to offset the toward-wave veering of the mean drag force. This phenomenon is discussed in this section.

We shall begin with presenting some typical predictions of current velocity profiles. Here, we consider four predictions with different wave–current angles ($\phi_{\tau h} = 0^\circ$, 30°, 60° and 90°), which share the same non-dimensional parameter set ($Re_* = 500$, $ad = 0.02$, $\hat{a} = 1$, $\hat{u}_w = 3$ and $\hat{S} = 1$). The veering of the current is given by the angle between the current velocity and the driving force, i.e. $\Delta\phi = \phi_{wc} - \phi_{\tau h}$, where ϕ_{wc} is the direction of current velocity. The oscillatory velocity is along the axis of $\phi_{wc} = 0$, and $\phi_{\tau h}$ is between 0 and 90°, so a positive $\Delta\phi$ means the velocity vector veers away from the axis of the oscillatory flow. As shown in figure 8(*a*), the reduction of current velocity magnitude decreases with $\phi_{\tau h}$, this is because a larger ϕ_{wc} (due to a larger $\phi_{\tau h}$) gives a smaller drag amplification factor and hence allows a larger current velocity. The value of $\Delta\phi$ is 0 for collinear ($\phi_{\tau h}$) and perpendicular ($\phi_{\tau h}$) wave–current flows in our model. For $\phi_{\tau h} = 30^\circ$ and 60°, $\Delta\phi$ increases from less than 5° at the canopy top to approximately 11° and 17° at the bottom, respectively. In the lower part of the canopy ($\hat{z} < 0.5$), where shear stress is negligible and the current velocity is almost uniform, the mean drag force balances the mean pressure gradient, so a uniform away-from-wave veering of current velocity vector is established to offset the towards-wave veering of drag. For instance, the $\Delta\phi = 11^\circ$ in the $\phi_{\tau h} = 60^\circ$ case gives a $\phi_{wc} = 71^\circ$ in the lower part of the canopy. The wave–current ratio $\alpha = U_w/|\boldsymbol{u}_c|$ is approximately 2 locally, so the towards-wave veering of the mean drag is approximately -10° (see figure 2), which just offsets the $\Delta\phi$.

To illustrate the effects of the canopy density, relative wave strength and submergence, here, we compare the predictions of $\phi_{\tau h} = 45^\circ$ wave–current flows with $Re_* = 500$, $ad = 200$. We tested $\hat{a} = [1, 5]$ and $\hat{S} = [1, 1/3]$, so a total of eight predictions are provided in figure 9. The following two remarks can be made.

https://doi.org/10.1017/jfm.2022.293 Published online by Cambridge University Press

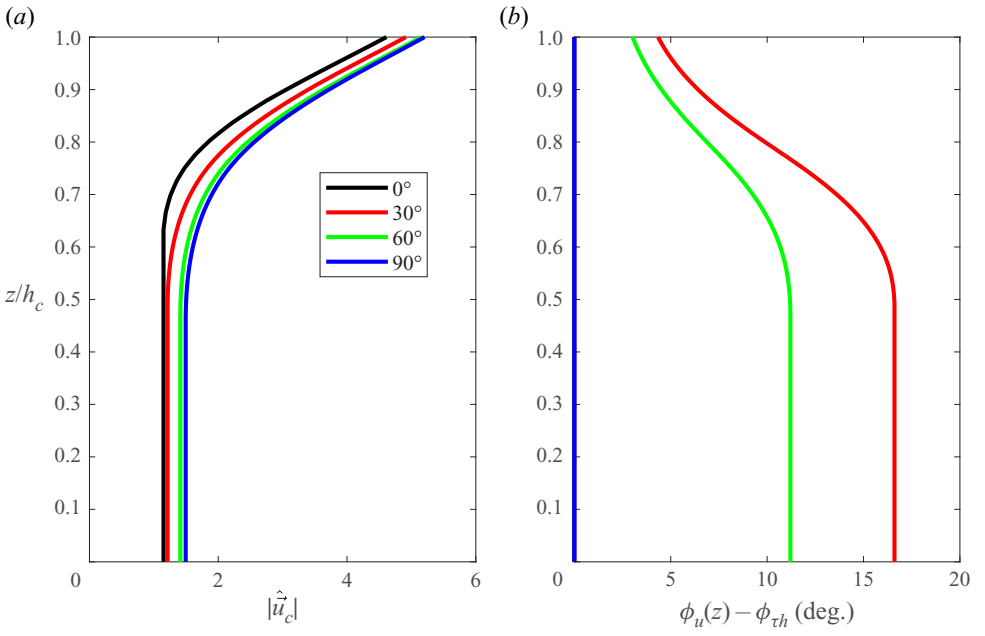


Figure 8. Vertical profiles of current velocity magnitude and veering of current direction for different wave–current angles. In all predictions: $Re_* = 500$, $ad = 0.02$, $\hat{a} = 1$, $\hat{u}_w = 3$ and $\hat{S} = 1$. (*a*) Current velocity. (*b*) Veering of current direction.

(i) Increasing relative wave strength increases the veering of current (the comparison between red and black lines in figure 9*b*,*d*).
(ii) Increasing the canopy solidity increases the veering of current (the comparisons between the dashed and solid lines in figure 9*b*,*d*).

These two remarks can be interpreted by considering the wave–current ratio, α. A larger relative wave strength directly increases α. A denser canopy will lead to weaker in-canopy current, $\hat{\boldsymbol{u}}_c$ under a prescribed driving force, since the penetration of overlying flow into the canopy is hindered. Thus, under the same wave velocity $\hat{u}_w$, the ratio $\alpha = |\hat{u}_w/\hat{\boldsymbol{u}}_c|$ is increased. As shown in figure 2, the veering angle increases with α, so the two remarks are explained.

The effect of submergence (the comparison between figure 9*b*,*d*) appears to be less significant. Reducing $\hat{S}$ leads to a weaker $|\hat{\boldsymbol{u}}_c|$ (compare figure 9*a*,*c*). This is because $\hat{S}$ is balanced by canopy drag in the near-bed region, so $\hat{S}$ is proportional to $|\hat{\boldsymbol{u}}_c|^2$. Reducing $\hat{S}$ from 1 to 1/3 would reduce $|\hat{\boldsymbol{u}}_c|$ by a factor of 0.58. This is not a huge reduction, so α and hence the veering angle is not changed a lot. If we were to compare very deep submergence ($\hat{S} \to 0$) with very shallow submergence ($\hat{S} \to \infty$), the difference could become much bigger.

The veering angle of the mean drag vector becomes independent of α for $\alpha > 10$, i.e. the contours in figure 2(*b*) becomes almost vertical at $\alpha = 10$, and the largest veering angle is slightly above 20° for ϕ_{wc} around 55°. Thus, it can be expected that the veering of in-canopy current has an upper limit around 20°. For instance, the cases with $\hat{a} = 5$ (dense canopy) and $\hat{u}_w = 3$ (strong wave) in figure 9 (the red dashed lines) have $\Delta\phi$ slightly over 20°.

https://doi.org/10.1017/jfm.2022.293 Published online by Cambridge University Press

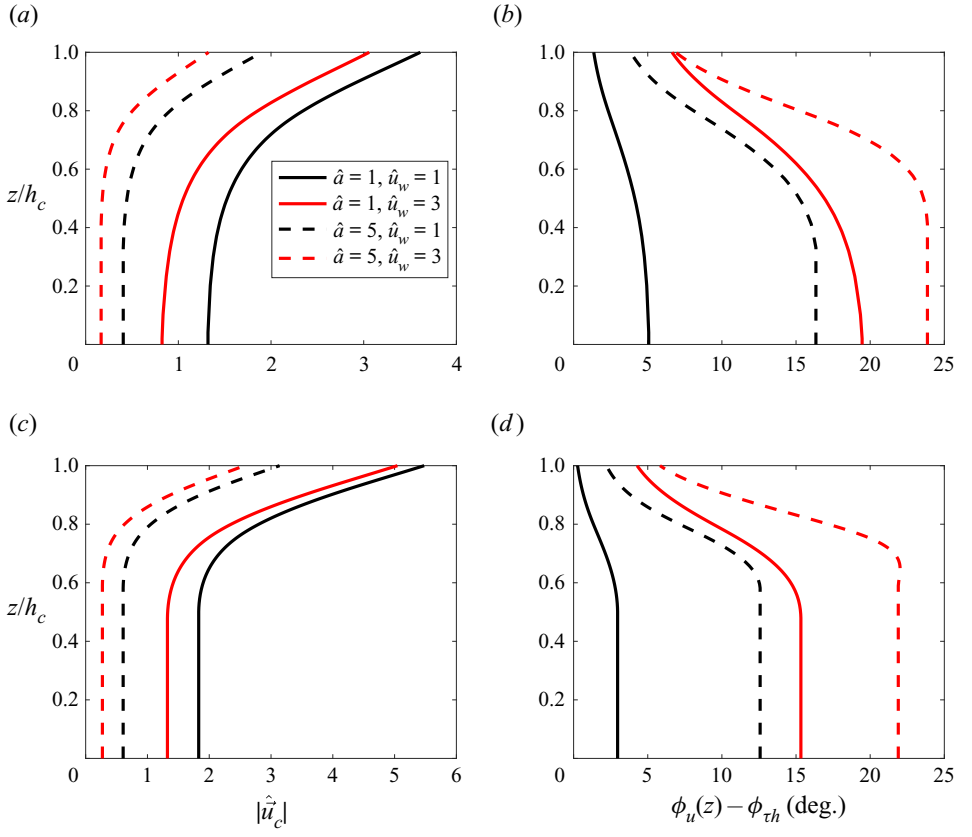


Figure 9. The effect of the canopy density, relative wave strength and submergence on wave–current canopy flows ((*a*,*c*) profiles of current velocity magnitude, (*b*,*d*) profiles of current veering). (*a*) Current velocity, deep submergence $\hat{S} = 1/3$. (*b*) Veering of current direction, deep shallow submergence $\hat{S} = 1/3$. (*c*) Current velocity, shallow submergence $\hat{S} = 1$. (*d*) Veering of current direction, shallow submergence $\hat{S} = 1$.

5. Conclusions

In this study, a one-dimensional semi-analytical model is developed for the current velocity profile inside a dense submerged canopy, which can account for a co-existing oscillatory flow driven by waves. The current is defined by two driving forces, the mean shear stress at the canopy top and the mean horizontal pressure gradient. The wave is simplified as a depth-uniform oscillatory flow. The canopy is assumed to be dense enough to have a lower layer in which the mean pressure gradient is mostly balanced by the mean drag force and hence has a quite depth-uniform current velocity. The model adopts a simple algebraic turbulence eddy viscosity model, which characterizes the mixing of momentum due to the strong shear-induced turbulence (i.e. the KH vortex) at the canopy top. The shear-related eddy viscosity is zero at the bottom, and increases linearly with elevation to a maximum value at the canopy top, which is proportional to the product of the current shear velocity and the penetration depth. The mean drag force is given by time averaging the instantaneous drag force given by a quadratic drag, which is widely used for the in-line force on a circular cylinder under wave–current flows. The nonlinearity of the quadratic law, i.e. $\overline{|\boldsymbol{u}(z,t)|\boldsymbol{u}(z,t)}$ does not equal to $\overline{|\boldsymbol{u}_c(z)|\boldsymbol{u}_c(z)}$, gives rise to a wave–current

https://doi.org/10.1017/jfm.2022.293 Published online by Cambridge University Press

interaction. Through normalization, it is found that the system is controlled by the direction of driving force and five normalized parameters: $\hat{a}$ ($= ah_c$, canopy density), $\hat{u}_w$ ($= U_w/u_{*c}$, relative wave strength), ad (canopy solid volume fraction), Re_* ($= u_{*c}d/\nu$, Reynolds number), $\hat{S}$ ($= gh_cS/u_{*c}^2$, the mean pressure gradient). The in-canopy current is solved numerically using a finite-volume method, while the analytical solutions of out-of-canopy current are provided.

The only model parameter, which is the scaling constant, c_s, of the shear-related eddy viscosity, is calibrated based on a set of unidirectional flume experiments of submerged dense canopies. It is found that c_s has a strong dependency on the submergence of the canopy. It is hypothesized that the behaviours of the KH vortex can be altered by a small depth of the above-canopy flow. Due to the lack of experimental data, we simply proposed a three-leg structure for c_s. The model is subsequently applied to a set of recent wave–current flume tests by Chen *et al.* (2020). It is shown that the model can accurately predict the in-canopy current profiles. The average model error for the entire in-canopy flow is a few per cent. In the very near-bottom region, where a uniform current velocity is expected, the error is approximately 10 %, but can be higher for low solidity and large wave conditions. This larger error possibly originates from the depth-uniform assumption of wave velocity. Nevertheless, the main effect of waves, i.e. retarding the in-canopy current, is well captured.

In this study, the wave effect amplifies the current's ability in producing a mean canopy drag force. A drag amplification factor, $\beta_c = |\overline{|\boldsymbol{u}_c(z)|\boldsymbol{u}_c(z)}|/|\boldsymbol{u}_c(z)|^2$, is introduced. It is found that the magnitude of β_c can far exceeds 1 if the wave velocity is comparable to or larger than the current velocity. Under the same current driving force, the total mean canopy drag force must be the same, so the current velocity in a wave–current flow has to be significantly reduced from that in a pure-current flow, in order to offset a large amplification factor. Therefore, it appears that waves retard the in-canopy current. For collinear wave–current flows, the reduction of the depth-averaged in-canopy current velocity increases with canopy density and wave strength. For wave and current at an angle, the mean drag vector veers towards the axis of oscillatory flows. In order to make a mean drag aligned with the direction of current driving force, the current velocity vector has to veer away from the axis of oscillatory flows. The veering angle of the drag vector is maximized for a wave–current angle around $30 \sim 60^\circ$, and it increases with the wave–current ratio. The largest veering angle is limited to around 20°. Thus, for wave–current flow over a dense canopy, the current velocity vector can veer from the direction of current driving force by up to 20°.

The model developed in this study is for an idealized condition, so the model is limited by the assumptions presented in table 1. Briefly speaking, our model is limited to the following.

(i) Idealized canopy: uniform cylindrical rods that is submerged and sufficiently dense.
(ii) Idealized wave: depth-uniform oscillatory flow that is not affected by current.
(iii) Idealized current: 1-DV problem.

Another contribution of this study is the simple parameterization of the turbulent eddy viscosity within the canopy. As previously mentioned, additional model calibration is required to further quantify how submergence affects the model parameter, c_s, of the shear-related eddy viscosity. Beside this, there are many other research questions that must be addressed to enable the model for field applications, such as

(i) adding a wave-induced mean flow in the model;

https://doi.org/10.1017/jfm.2022.293 Published online by Cambridge University Press

(ii) studying how flexibility and the heterogeneity of the canopy affect the in-canopy drag;
(iii) studying whether the KH vortices can be modified by co-existing waves and (if so) adding the wave influence in the formulation of shear-related turbulent eddy viscosity;
(iv) studying the effect of currents on waves and adding a wave component to the model.

Due to the complexity of coastal flows and aquatic canopies, there can be other mechanisms of wave–current interaction beyond this list. Lots of future research efforts, especially for high-quality field and laboratory observations, are required to close these knowledge gaps and to develop predictive model for field applications.

Acknowledgement. We would like to acknowledge the three anonymous referees for their comments and suggestions, which substantially improved the quality of the paper.

Funding. This work was supported by the Fund Program of State Key Laboratory of Hydroscience and Engineering (grant number 2022-KY-05)/(2022-KY-05).

Declaration of interests. The authors report no conflict of interest.

Author ORCIDs.
Weikai Tan https://orcid.org/0000-0001-9083-7418;
Jing Yuan https://orcid.org/0000-0002-6866-5178.

Appendix A. Numerical solution of in-canopy current

The entire canopy, i.e. $0 \le \hat{z} \le 1$, is discretized into N nodes with a uniform internal $\Delta\hat{z}$. The first node is $\hat{z} = 0$, and the last node is $\hat{z} = 1$. The normalized current velocity and shear stress at the first node is given by the boundary condition, i.e.

$$\hat{u}_{cx,1} = \hat{u}_{0x}, \quad \hat{u}_{cy,1} = \hat{u}_{0y} \tag{A1a,b}$$

and

$$\hat{\tau}_{x,1} = \hat{\nu}_T \frac{\partial \hat{u}_{cx}}{\partial \hat{z}}\bigg|_1 = 0, \quad \hat{\tau}_{y,1} = \hat{\nu}_T \frac{\partial \hat{u}_{cy}}{\partial \hat{z}}\bigg|_1 = 0. \tag{A2a,b}$$

The solutions at the remaining nodes are determined in sequence. Here, we consider two nodes n and $n+1$. We also denote the midpoint between the two nodes as node $n+0.5$. The task is to find flow velocity and the shear stress at node $n+1$. The difference of velocity between the two nodes is denoted as

$$(\Delta\hat{u}_x, \Delta\hat{u}_y) = (\hat{u}_{cx,n+1} - \hat{u}_{cx,n}, \hat{u}_{cy,n+1} - \hat{u}_{cy,n}). \tag{A3}$$

We consider a control volume between the two nodes. The momentum balance of this control volume can be written as

$$\hat{\tau}_{i,n+1} - \hat{\tau}_{i,n} = (\bar{f}_{di,n+0.5} - \hat{S}_i)\Delta\hat{z}, \quad i = x, y. \tag{A4}$$

The drag at the midpoint is

$$\bar{f}_{di,n+0.5} = \frac{1}{2}\hat{a}\beta_{ci,n+0.5}C_{D,n+0.5}(\hat{u}_{ci,n} + \Delta\hat{u}_i/2)^2, \quad i = x, y. \tag{A5}$$

The shear stress at the midpoint is

$$\hat{\tau}_{i,n+0.5} = \hat{\nu}_{T,n+0.5}\frac{\Delta\hat{u}_i}{\Delta\hat{z}} = \frac{\hat{\tau}_{i,n+1} + \hat{\tau}_{i,n}}{2}, \quad i = x, y. \tag{A6}$$

https://doi.org/10.1017/jfm.2022.293 Published online by Cambridge University Press

Thus, the left-hand side of (A4) can be written as

$$\hat{\tau}_{i,n+1} - \hat{\tau}_{i,n} = 2(\hat{\tau}_{i,n+0.5} - \hat{\tau}_{i,n}) = 2\hat{\nu}_{T,n+0.5}\frac{\Delta\hat{u}_i}{\Delta\hat{z}} - 2\hat{\tau}_{i,n}, \quad i = x, y. \tag{A7}$$

By substituting (A5) and (A7) into (A4), the following equation for $\Delta\hat{u}_i$ is obtained:

$$\Delta\hat{u}_i = \frac{1}{2\hat{\nu}_{T,n+0.5}}\left[2\hat{\nu}_{T,n}\left.\frac{\partial\hat{u}_{ci}}{\partial\hat{z}}\right|_n \Delta\hat{z} + \left(\frac{1}{2}\hat{a}\beta_{ci,n+0.5}C_{D,n+0.5}(\hat{u}_{ci,n} + \Delta\hat{u}_i/2)^2 - \hat{S}_i\right)\Delta\hat{z}^2\right], \quad i = x, y. \tag{A8}$$

Since $\Delta\hat{u}_i$ appears on both sides, this equation can be iteratively solved to give $\Delta\hat{u}_i$. The shear stress at node $n + 1$ is subsequently evaluated via

$$\hat{\tau}_{i,n+1} = \hat{\nu}_{T,n+1}\left.\frac{\partial\hat{u}_{ci}}{\partial\hat{z}}\right|_{n+1} = \hat{\tau}_{i,n} + \left(\frac{1}{2}\hat{a}\beta_{ci,n+0.5}C_{D,n+0.5}(\hat{u}_{ci,n} + \Delta\hat{u}_i/2)^2 - \hat{S}_i\right)\Delta\hat{z}, \quad i = x, y. \tag{A9}$$

References

Abdolahpour, M., Hambleton, M. & Ghisalberti, M. 2017 The wave-driven current in coastal canopies. *J. Geophys. Res.: Oceans* **122** (5), 3660–3674.

Adams, M.P., Ghisalberti, M., Lowe, R.J., Callaghan, D.P., Baird, M.E., Infantes, E. & O'Brien, K.R. 2018 Water residence time controls the feedback between seagrass, sediment and light: implications for restoration. *Adv. Water Resour.* **117**, 14–26.

Carpenter, R.C., Hackney, J.M. & Adey, W.H. 1991 Measurements of primary productivity and nitrogenase activity of coral reef algae in a chamber incorporating oscillatory flow. *Limnol. Oceanogr.* **36** (1), 40–49.

Chen, M., Lou, S., Liu, S., Ma, G., Liu, H., Zhong, G. & Zhang, H. 2020 Velocity and turbulence affected by submerged rigid vegetation under waves, currents and combined wave–current flows. *Coast. Engng* **159**, 103727.

Donatelli, C., Ganju, N.K., Fagherazzi, S. & Leonardi, N. 2018 Seagrass impact on sediment exchange between tidal flats and salt marsh, and the sediment budget of shallow bays. *Geophys. Res. Lett.* **45** (10), 4933–4943.

Dupont, S. & Brunet, Y. 2009 Coherent structures in canopy edge flow: a large-eddy simulation study. *J. Fluid Mech.* **630**, 93–128.

Falter, J.L., Atkinson, M.J. & Coimbra, C.F.M. 2005 Effects of surface roughness and oscillatory flow on the dissolution of plaster forms: evidence for nutrient mass transfer to coral reef communities. *Limnol. Oceanogr.* **50** (1), 246–254.

Ferrario, F., Beck, M.W., Storlazzi, C.D., Micheli, F., Shepard, C.C. & Airoldi, L. 2014 The effectiveness of coral reefs for coastal hazard risk reduction and adaptation. *Nat. Commun.* **5** (1), 1–9.

Fonseca, M.S. & Cahalan, J.A. 1992 A preliminary evaluation of wave attenuation by four species of seagrass. *Estuar. Coast. Shelf Sci.* **35** (6), 565–576.

Ghisalberti, M. 2009 Obstructed shear flows: similarities across systems and scales. *J. Fluid Mech.* **641**, 51–61.

Ghisalberti, M. & Nepf, H.M. 2004 The limited growth of vegetated shear layers. *Water Resour. Res.* **40** (7), W07502.

Ghisalberti, M. & Nepf, H.M. 2002 Mixing layers and coherent structures in vegetated aquatic flows. *J. Geophys. Res.: Oceans* **107** (C2), 3-1–3-11.

Ghisalberti, M. & Schlosser, T. 2013 Vortex generation in oscillatory canopy flow. *J. Geophys. Res.: Oceans* **118** (3), 1534–1542.

Grant, W.D. & Madsen, O.S. 1979 Combined wave and current interaction with a rough bottom. *J. Geophys. Res.: Oceans* **84** (C4), 1797–1808.

Grant, W.D. & Madsen, O.S. 1986 The continental-shelf bottom boundary layer. *Annu. Rev. Fluid Mech.* **18** (1), 265–305.

https://doi.org/10.1017/jfm.2022.293 Published online by Cambridge University Press

HU, Z., SUZUKI, T., ZITMAN, T., UITTEWAAL, W. & STIVE, M. 2014 Laboratory study on wave dissipation by vegetation in combined current–wave flow. *Coast. Engng* **88**, 131–142.

HURD, C.L. 2000 Water motion, marine macroalgal physiology, and production. *J. Phycol.* **36** (3), 453–472.

KING, A.T., TINOCO, R.O. & COWEN, E.A. 2012 A k-[epsilon] turbulence model based on the scales of vertical shear and stem wakes valid for emergent and submerged vegetated flows. *J. Fluid Mech.* **701**, 1–39.

LI, C.W. & YAN, K. 2007 Numerical investigation of wave–current–vegetation interaction. *ASCE J. Hydraul. Engng* **133** (7), 794–803.

LOU, S., CHEN, M., MA, G., LIU, S. & ZHONG, G. 2018 Laboratory study of the effect of vertically varying vegetation density on waves, currents and wave-current interactions. *Appl. Ocean Res.* **79**, 74–87.

LOWE, R.J., KOSEFF, J.R. & MONISMITH, S.G. 2005 Oscillatory flow through submerged canopies: 1. Velocity structure. *J. Geophys. Res.: Oceans* **110**, C10016.

LUHAR, M., COUTU, S., INFANTES, E., FOX, S. & NEPF, H. 2010 Wave-induced velocities inside a model seagrass bed. *J. Geophys. Res.: Oceans* **115**, C12005.

LUHAR, M., INFANTES, E. & NEPF, H. 2017 Seagrass blade motion under waves and its impact on wave decay. *J. Geophys. Res.: Oceans* **122** (5), 3736–3752.

LUHAR, M., INFANTES, E., ORFILA, A., TERRADOS, J. & NEPF, H.M. 2013 Field observations of wave-induced streaming through a submerged seagrass (posidonia oceanica) meadow. *J. Geophys. Res.: Oceans* **118** (4), 1955–1968.

MA, G., KIRBY, J.T., SU, S.-F., FIGLUS, J. & SHI, F. 2013 Numerical study of turbulence and wave damping induced by vegetation canopies. *Coast. Engng* **80**, 68–78.

MAZA, M., LARA, J.L. & LOSADA, I.J. 2013 A coupled model of submerged vegetation under oscillatory flow using Navier–Stokes equations. *Coast. Engng* **80**, 16–34.

MENDEZ, F.J. & LOSADA, I.J. 2004 An empirical model to estimate the propagation of random breaking and nonbreaking waves over vegetation fields. *Coast. Engng* **51** (2), 103–118.

MONTI, A., OMIDYEGANEH, M., ECKHARDT, B. & PINELLI, A. 2020 On the genesis of different regimes in canopy flows: a numerical investigation. *J. Fluid Mech.* **891**, A9.

NEPF, H.M. 2012 Flow and transport in regions with aquatic vegetation. *Annu. Rev. Fluid Mech.* **44**, 123–142.

NEPF, H.M. & VIVONI, E.R. 2000 Flow structure in depth-limited, vegetated flow. *J. Geophys. Res.: Oceans* **105** (C12), 28547–28557.

ONDIVIELA, B., LOSADA, I.J., LARA, J.L., MAZA, M., GALVÁN, C., BOUMA, T.J. & VAN BELZEN, J. 2014 The role of seagrasses in coastal protection in a changing climate. *Coast. Engng* **87**, 158–168.

RAUPACH, M.R., FINNIGAN, J.J. & BRUNET, Y. 1996 Coherent eddies and turbulence in vegetation canopies: the mixing-layer analogy. *Boundary-Layer Meteorol* **78**, 351–382.

REIDENBACH, M.A., KOSEFF, J.R. & KOEHL, M.A.R. 2009 Hydrodynamic forces on larvae affect their settlement on coral reefs in turbulent, wave-driven flow. *Limnol. Oceanogr.* **54** (1), 318–330.

VAN ROOIJEN, A., LOWE, R., RIJNSDORP, D.P., GHISALBERTI, M., JACOBSEN, N.G. & MCCALL, R. 2020 Wave-driven mean flow dynamics in submerged canopies. *J. Geophys. Res.: Oceans* **125** (3), e2019JC015935.

SARPKAYA, T. & STORM, M. 1985 In-line force on a cylinder translating in oscillatory flow. *Appl. Ocean Res.* **7** (4), 188–196.

SUZUKI, T., ZIJLEMA, M., BURGER, B., MEIJER, M.C. & NARAYAN, S. 2012 Wave dissipation by vegetation with layer schematization in swan. *Coast. Engng* **59** (1), 64–71.

TANINO, Y. & NEPF, H.M. 2008*a* Laboratory investigation of mean drag in a random array of rigid, emergent cylinders. *ASCE J. Hydraul. Engng* **134** (1), 34–41.

TANINO, Y. & NEPF, H.M. 2008*b* Lateral dispersion in random cylinder arrays at high Reynolds number. *J. Fluid Mech.* **600**, 339–371.

TINOCO, R.O. & COCO, G. 2018 Turbulence as the main driver of resuspension in oscillatory flow through vegetation. *J. Geophys. Res.: Earth Surf.* **123** (5), 891–904.

TSCHISGALE, S., LÖHRER, B., MELLER, R. & FRÖHLICH, J. 2021 Large eddy simulation of the fluid-structure interaction in an abstracted aquatic canopy consisting of flexible blades. *J. Fluid Mech.* **916**, A43.

VIANA PARENTE LOPES, J.M., PALMA, J.M.L.M. & SILVA LOPES, A. 2021 Modelling the flow within forests: the canopy-related terms in the Reynolds-averaged formulation. *J. Fluid Mech.* **910**, A7.

WARD, L.G., KEMP, W.M. & BOYNTON, W.R. 1984 The influence of waves and seagrass communities on suspended particulates in an estuarine embayment. *Mar. Geol.* **59** (1-4), 85–103.

WEITZMAN, J.S., ZELLER, R.B., THOMAS, F.I.M. & KOSEFF, J.R. 2015 The attenuation of current- and wave-driven flow within submerged multispecific vegetative canopies. *Limnol. Oceanogr.* **60** (6), 1855–1874.

https://doi.org/10.1017/jfm.2022.293 Published online by Cambridge University Press

YANG, J.Q. & NEPF, H.M. 2018 A turbulence-based bed-load transport model for bare and vegetated channels. *Geophys. Res. Lett.* **45** (19), 10–428.

YUAN, J. & MADSEN, O.S. 2015 Experimental and theoretical study of wave-current turbulent boundary layers. *J. Fluid Mech.* **765**, 480–523.

ZELLER, R.B., ZARAMA, F.J., WEITZMAN, J.S. & KOSEFF, J.R. 2015 A simple and practical model for combined wave–current canopy flows. *J. Fluid Mech.* **767**, 842–880.

ZHANG, Y., TANG, C. & NEPF, H. 2018 Turbulent kinetic energy in submerged model canopies under oscillatory flow. *Water Resour. Res.* **54** (3), 1734–1750.

ZHOU, C.Y. & GRAHAM, J.M.R. 2000 A numerical study of cylinders in waves and currents. *J. Fluids Struct.* **14** (3), 403–428.

ZHOU, J. & VENAYAGAMOORTHY, S.K. 2019 Near-field mean flow dynamics of a cylindrical canopy patch suspended in deep water. *J. Fluid Mech.* **858**, 634–655.

https://doi.org/10.1017/jfm.2022.293 Published online by Cambridge University Press